

AD-A262 380



15

EXPLORATION OF MULTILAYER CONCEPTS FOR
OXIDATION PROTECTION OF CARBON-CARBON COMPOSITES

R. V. SARA

UCAR CARBON COMPANY INC.
12900 SNOW ROAD
PARMA, OHIO 44130

FEBRUARY, 1993

FINAL REPORT
CONTRACT NO. N00014-90-C-0057/P00002

Reproduced From
Best Available Copy

PREPARED FOR:

A. JOHN SEDRIKS - ONR SCIENTIFIC OFFICER
OFFICE OF NAVAL RESEARCH
DEPARTMENT OF THE NAVY
ARLINGTON, VIRGINIA 22217

20000920330

93 3 10 047

DTIC
SELECTED
MAR 30 1993
S B D

DISTRIBUTION STATEMENT A
Approved for public release;
Distribution Unlimited

93-05166



7488

TABLE OF CONTENTS

	<u>Page</u>
ABSTRACT	1
INTRODUCTION	2
EXPERIMENTAL	3
A. Substrates	4
B. Compliant Layers	5
C. Diffusion Layers	6
D. Erosion Protection	8
E. Fabrication	9
F. Laser Fusion	11
G. Materials	12
H. Coating Configurations	12
I. Evaluations	14
RESULTS AND DISCUSSION	14
Microstructural Evaluations	14
Compliant Layer Properties	18
Oxidation Results	19
CONCLUSIONS	21
SUMMARY AND RECOMMENDATIONS	23
REFERENCES	25
APPENDIX	26
Table II	27
Table IIIA, B, C, D, E, F	29
Table IV	34
Table VA, B, C, D, E, F	37
Table VI	42
Figures 1-25	44
DISTRIBUTION LIST	69

EXPLORATION OF MULTILAYER CONCEPTS FOR OXIDATION PROTECTION OF CARBON-CARBON COMPOSITES

by

R. V. SARA
UCAR CARBON COMPANY INC.
12900 SNOW ROAD
PARMA, OHIO 44130

ABSTRACT

The development of multilayer coating concepts for oxidation protection of carbon-carbon composites is the subject of this work. Property requirements of constituents for candidate systems are presented. In this regard, erosion, carbon and oxygen diffusion, chemical stability, bonding, compliancy and thermal expansion are discussed and the impact they have on coating effectiveness is correlated with experimental coating results. Of particular interest is the ability to manipulate crack origin, propagation direction and stoppage by giving judicious consideration to layer CTE and compliance. This capability increases the opportunity to fabricate multilayer coatings with crack-free oxygen diffusion layers. Chemical vapor deposited SiC on compliant substrates was essentially crack-free and, therefore, provided excellent oxidation protection.

1982 OCT 10 10 10 AM 1

Accession For	
NTIS GRA&I	<input checked="checked" type="checkbox"/>
DTIC TAB	<input type="checkbox"/>
Unannounced	<input type="checkbox"/>
Justification	
By <i>per letter</i>	
Distribution/	
Availability Codes	
Dist	Avail and/or Special
<i>A-1</i>	

INTRODUCTION

Carbon/carbon composites (CC) have received considerable attention in the aerospace industry for a variety of applications requiring strength, stiffness, toughness and low weight. However, the fact that CC commences to oxidize at about 930°F (500°C) places a severe limitation on the use of these composites where the carbon might react with oxygen. In order to circumvent the oxidation problem, it is recognized that efficient coating systems are required to protect the composites.

Work directed toward protecting graphite has been in progress for more than fifty years as evidenced by patents issued in that time period. Efforts to develop protective coatings for CC were initiated in the early 1970's. The principal problem with coating CC has been its very low thermal expansion relative to most refractory materials. Hence, Si_3N_4 and SiC , which come closest to being strain compatible, have been shown to provide good protection to approximately 3000°F (1650°C) for reasonable time periods.⁽¹⁾ Boron-rich inner layers have helped the protective capability of Si_3N_4 and SiC by sealing microcracks which typically form in these coatings. However, these layers are moisture sensitive, and may cause destruction of the coating by rapid moisture release. Furthermore, conditions which favor SiO formation and volatility are known to adversely impact protective lifetimes and operation temperatures.⁽²⁾

The protection of CC for long time periods at temperatures above 3270°F (1800°C) is a very formidable task and requires concepts much different from those described above. It has been recognized⁽³⁾ for some time that carbon and oxygen diffusion through the coating material are important phenomena. To function adequately as a protective layer, the coating volatility must be low, particularly in environments of reduced pressures and high

temperatures. Adherence between coating and substrate will be governed by chemical stability in the presence of oxygen and carbon and by mechanical compatibility. It is unlikely that a single coating material would have all these chemical and mechanical requirements.

Multilayer systems have been proposed⁽⁴⁾⁽⁵⁾ whereby discrete layers would have functions such as carbon diffusion barriers (carbides, Iridium), oxygen diffusion barriers (SiO_2 , Iridium) erosion barriers (oxides). In addition, attention would have to be given to the thermal expansion mismatches, bond strength between coating and substrate, as well as layer thicknesses. The overall concept has been utilized very little because the fabricating processes required to achieve dense, graded, multicomponent systems is a challenging undertaking.

The purpose of the present work is to develop new concepts for oxidation protection of CC composites with emphasis on multilayer systems and particularly on the use of compliant layers to accommodate stresses arising from the thermal expansion mismatch between substrate and coating components. Since elevated temperature properties were lacking for many components, the study was relegated to fabrication and assessment rather than one based on analytical considerations. However, special consideration was given to thermal expansion and the effect this had on structural integrity was carefully analyzed.

EXPERIMENTAL

The materials criteria and procedures adapted for synthesizing numerous multilayer systems are described in subsequent sections. As mentioned previously, the objective of this effort was to

develop multilayer concepts for the oxidation protection of CC composites.

An effective multilayer coating system has certain important criteria which are identified in the highly documented Figure 1. The layers in this scheme function as carbon or oxygen diffusion barriers, they provide erosion protection, compliancy, adherence, and chemical stability. They are strategically stacked with respect to the substrate to most effectively serve in their intended capacity. Another important aspect of the multilayers is to reduce thermomechanical strains in the overall coating. This is achieved in part by grading the constituent layers, not only in terms of function, but in terms of their thermal expansion coefficients. The thermal expansion mismatch between virtually all coating materials and CC has caused cracks to form in the coating thereby preventing the implementation of coated CC in hot oxidizing environments.

A. Substrates

The substrates used in this work, CC and monolithic graphite, have low thermal expansion coefficients (CTE). The former were grades STC2 and ACC-4 provided by B. F. Goodrich Company and LTV Missiles and Electronics Division, respectively. Both CC materials were two-dimensional lay up, uninhibited with the thicknesses of 1/4" and 3/16". The monolithic graphite was UCAR Grade ATJ fine-grain graphite. This material has a thermal expansion coefficient of $4.0 \times 10^{-6} \text{ } ^\circ\text{C}^{-1}$ over the temperature range 75°-1830°F (25°-1000°C), a value which is orders of magnitude higher than CC composites, but much less than the oxides and carbides considered as diffusion barriers in this effort.

B. Compliant Layers

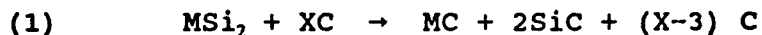
Compliant layers were employed to help accommodate stresses developed between the substrate and the constituent layers as a result of CTE differences. The low modulus compliant layers included pyrolytic graphite (PG), pyrolytic graphite coating (PGC), pitch/graphite mixtures, carbide/graphite and carbide mixtures.

The pyrolytic graphite coating on ATJ graphite was approximately 65 μm thick. Both PG and PG coating substrates were found to delaminate easily. Furthermore, adhesion between the PG type substrates and adjoining layers frequently was poor. Hence, PG-type compliant materials received limited consideration.

A proprietary pitch/20 w/o graphite mixture as a compliant layer required multiple applications and firings to 930°F (500°C) in order to obtain a continuous coating as shown in Figure 2(A). Large graphite flakes up to 20 μm in length are evident in this coating. There was a strong tendency for the flakes to orient with their basal planes parallel to the substrate.

A different coating shown in 2(B) is based on a proprietary pitch/20 w/o lampblack mixture. It can be seen that the coating features finely dispersed particles in the pitch matrix. Seemingly, the lampblack contributed to a higher CTE coating as evidenced by microcrack formations. This compliant coating concept was pursued only to a limited degree because multiple applications and firings seemed impractical.

Compliant layers consisting of ternary mixtures such as $\text{HfC} + \text{SiC} + \text{graphite}$ were prepared by reacting HfSi_2 or an appropriate disilicide with graphite. Free graphite coexists with SiC and MC when X exceeds 3 in the following equation:



Experimental work established that a TiSi_2 based reaction commenced at 2460°F (1350°C) with liberation of Si. The Si penetrates graphite and CC, providing the latter does not have a thin PG coating. Molten Si ultimately reacts with the carbon to form SiC. The reaction involving HfSi_2 occurs at 2250°F (1400°C). A flake-type graphite designated UCAR GP-39 was used in these preparations; particles were -35 μm . It was necessary to hot press all compliant layer mixtures containing GP-39.

Test bars (0.25" x 0.40" x 2.5") for physical property measurements were prepared by hot pressing HfSi_2 +XC mixtures at 3360°F (1850°C). The values for X were 3, 5, 7 and 9. After the reaction, excess moles of graphite were 0, 2, 4 and 6, respectively. Property measurements contemplated for these specimens included bulk density, Young's modulus and thermal expansion.

A compliant layer for CVD SiC was applied to graphite and CC by reacting TiSi_2 +XC slurry mixtures on their surfaces. Values for X ranged between 0 and 0.5 or less than one mole carbon. Thus, the compliant layers would not feature free graphite. The reactions were done at 2920°F (1550°C).

C. Diffusion Layers

Diffusion plays an important role in the high temperature protective ability of a multilayer system. It has been recognized that carbon diffusion to the exterior and oxygen diffusion inward are critical phenomenon that control carbon loss and coating integrity. The rate at which carbon is lost may be directly correlated with carbon penetration of the coating and subsequent

reaction on the outside with oxygen. Disruptive pressures could develop at the carbon interface as a result of carbon monoxide formed by the reaction between penetrated oxygen and carbon.

Various diffusion mechanisms are operative in a multilayer coating system. Published diffusion data must be considered carefully in view of microstructural, purity, and measurement differences. This is particularly true for materials containing pores or cracks because the diffusion rate is much faster than is diffusion through dense solids or single crystals. Grain boundary diffusion is another consideration because the rate is faster than it is in a homogeneous solid. CVD deposits frequently are columnar with the growth direction paralleling the carbon diffusion path. A direct grain boundary path such as this may have a marked effect on diffusion rates.

Nevertheless, some generalities can be drawn as evidenced by Figure 3. It can be seen that oxygen diffusion through ZrO_2 , HfO_2 , is relatively fast compared to Al_2O_3 , SiO_2 and Iridium. The latter has outstanding barrier qualities for both oxygen and carbon, but the scarcity and high thermal expansion of this metal have limited its use to extraordinary applications. The low oxygen diffusion rate through silica films is responsible for excellent oxidation characteristics of materials such as Si_3N_4 , SiC and $MoSi_2$. The limiting feature with SiO_2 is reduction to SiO and its subsequent vaporization. The thermodynamic processes of importance here have been well documented elsewhere.⁽⁶⁾

Several approaches were taken by us to reduce the conversion of SiO_2 to SiO . The first consisted of applying oxide covercoats such as HfO_2 , Y_2O_3 , Al_2O_3 , $3Y_2O_3 \cdot 5Al_2O_3$, $Y_2O_3 \cdot SiO_2$, $La_2O_3 \cdot 2ZrO_2$ over SiC diffusion barriers. The second approach involved use of binary refractory mixtures such as $HfB_2 + SiC$, $Al_2O_3 + MoSi_2$, etc.

The problem encountered with the various coverages was the creation of low melting oxide mixtures with relatively low viscosity. This condition was a deterrent to further investigation of these approaches.

Certain carbides and presumably borides are good carbon diffusion barriers. The carbide data plotted in Figure 4 substantiates in part the foregoing statement. It is apparent that carbon diffusion through HfC and TaC is several orders of magnitude slower than it is through lighter metal carbides like TiC. Silica and SiC are also excellent barrier materials. Furthermore, the carbides have extremely high melting temperatures and their eutectic temperatures with carbon are also very high. In this work, TaC, HfC, SiC and TiC were incorporated as carbon barriers in the multilayer systems.

D. Erosion Protection

Certain applications for coated CC composites include exposing them to high velocity hot particles and reduced ambient pressures where vaporization becomes a serious threat to lifetime. It is apparent, therefore, that hard ceramic outer coatings with low vapor pressures are required for these applications. The data shown in Table I are taken from Sheehan.⁽⁷⁾ Although the list of low vapor pressure erosion ceramics is relatively large, most can be excluded for one reason or another. The oxides HfO₂, Y₂O₃, ZrO₂ and Al₂O₃ are least objectionable from the standpoint of toxicity, radioactivity, hydrolysis and refractoriness. Therefore, they were employed as the outermost layer in numerous multilayer configurations prepared during this program.

Table I

Temperatures (°C) for Oxide Vapor Pressures of 10^{-3} mm

HfO ₂	Y ₂ O ₃	ThO ₂	ZrO ₂	BeO	Al ₂ O ₃	CaO	TiO ₂	SiO ₂	MgO
2475	2250	2239	2239	2027	1905	1875	1780	1770	1695
(a) 10^{-4} mm due to 2010°C melting point.									
(b) 10^{-4} mm due to 1838°C melting point.									

E. Fabrication

A variety of techniques were employed to prepare densified multilayer specimens for evaluation. The most common approach, however, consisted of painting glue-powder slurries as a layered array in a 3/4" diameter graphite mold lined with GRAFOIL™ and then hot pressing. Layer formulations on either side of the substrate were varied at times in order to expedite the number of pressed formulations. The graphite mold was heated inductively and temperatures were measured with an optical pyrometer. A stainless steel vacuum chamber housing the mold assembly was evacuated to 2 TORR at room temperature prior to purging with argon throughout the course of the run. Heating to pressing temperatures of 3360°F (1850°C) or 3580°F (2000°C) was done rapidly (20-30 minutes) and pressure was applied via double acting rams at temperature. Pressing times varied from 30 minutes to five hours.

Consolidation in the above manner was used in numerous instances where strain compatibility and chemical stability were of particular interest. Since specimen perimeter areas were uncoated because of pressure constraints, it is apparent oxidation tests could not be performed. Thus, two approaches were taken in an effort to densify all specimen surfaces. A quasi isostatic method was investigated as one alternative.⁽⁶⁾ The process had appeal because it could be adapted to our present hot press system and the

quick turn around was another important time factor. The drawing in Figure 5 illustrates the mold configuration, particularly the cut-a-way which contributed to greater coating thickness uniformity on the sides. The fluid coke ($\sim 150 \mu\text{m}$ diameter, a product of Superior Graphite Company) transmitted pressure to all surfaces, but microscopic studies ultimately revealed the sides were less dense than the top and bottom. Oxidation results were adversely affected by the density variations. The final attempt at densifying all surfaces involved three separate hot pressings of coated cube-shaped specimens. Although the six faces were densified in this method, the cube edges lacked sufficient structural integrity to prevent rapid oxygen ingress.

The hot isostatic pressing (HIP) technique was also used in our attempts to prepare high density uniformly coated specimens. The CC and ATJ coated specimens were clad in Niobium metal by Ed Gorsky at College Park, MD, and then pressed at AAB Autoclave Systems, Columbus, OH. The samples were pressed at 30,000 psi for one hour at 3360°F (1850°C). Defects of one form or other in the five coated specimens prevented oxidation testing. However, the fact that portions of quality coating tenaciously adhered to the substrates suggests additional work might be advisable.

Chemical vapor deposition (CVD) is used a great deal for applying a variety of dense coatings on graphite and CC. The most popular CVD coatings are SiC for oxidation protection of graphite and hard carbides such as TiC for cutting tool applications. A variety of nitrides such as BN, AlN, Si_3N_4 , borides like TiB_2 , HfB_2 , silicides, oxides and carbon are also part of the CVD list. We limited our deposited coatings to just a few examples because developing processes for complex multilayer systems is a formidable task and beyond the scope of this project.

Reaction-assisted sintering was used to a large degree during hot pressing as well as during pressureless sintering. The basis for this concept is equation (1) where it was indicated liquid silicon formed and subsequently reacted with carbon to produce SiC. This process helped densification by virtue of producing a liquid phase. Liquid was produced at all levels of the coating in pressureless sintering processes but its formation was confined to specific layers such as compliant ones when hot pressing was done.

The various layers of reaction sintered specimens such as 6-78 listed in Table IV were applied by air spraying or brushing slurries. The coating on 6-78 is multilayer and densified by a self reacting process. The layer 4 slurry mixture comprising $\text{TiSi}_2 + 3\text{w/oB}_4\text{C}$ and a high char yield proprietary binder was brushed on the ATJ surface. The second and third layers featuring $\text{TiSi}_2 + \text{Al}_2\text{O}_3$ and glue were also hand painted. The coated specimen then was heated to 3360°F (1850°C) for one hour. Afterward, a $\text{TiSi}_2/\text{glue}$ mixture was applied and the specimen was refired. Finally, an Al_2O_3 surface coating was applied by plasma spraying.

F. Laser Fusion

A series of experiments were conducted at Laser Automation, Inc., Chagrin Falls, Ohio, relative to reacting TiSi_2 , TaSi_2 , and HfSi_2 with monolithic ATJ graphite by laser heating. This concept of using a high energy laser to fuse coatings and substrates together has been practiced elsewhere.⁽⁹⁾ We also successfully employed the method at this facility to complete exchange reactions between a carbonaceous surface and intermetallics such as Al_3Ti . Relatively dense, well-bonded coatings were achieved. The experimental work at Laser Automation considered translation speeds, beam energies, spot configurations

and the effect of carbon additives. Best fusion results were obtained for HfSi_2 , applied as a flame sprayed coating on ATJ graphite. The photomicrograph in Figure 6(A) indicates considerable fusion and penetration of melt into the graphite had occurred. Analytical work by SEM and EDX revealed the white areas consisted of two phases with varying Si contents. The photograph in Figure 6(B) reveals a lamellar-like relationship between the two phases. Existence of chemical bonding is questionable. The outer layer is highly oxidized to HfO_2 , even though a shroud of argon was employed. Microcracks in the coating are also visible. The fact that graphite did not dissolve in the molten Hf/Si alloy raises a concern about lack of compliancy and structural integrity of this layer.

G. Materials

A relatively large number of powder materials were used in the fabrication work. These were used in the layering process as reactants, to prepare additional compounds, and as plasma spray powders. Data such as the source, grade, purity and particle size are presented in Table II. It can be seen that the information is incomplete in the grade category mainly because chemical houses do not use this classification term. Attempts were made to obtain and use the purest powders and finest particles possible.

H. Coating Configurations

A considerable number of multilayer configurations were prepared by hot pressing powders listed in Table II. A multitude of pressings was undertaken because turn-around time was relatively fast and evaluations were informative. The effect of a compliant layer on structural integrity of densified coatings was of paramount interest; however, influence of CTE's was also a major

concern. Thermochemical stability was evaluated and compared with published results.

The configuration in Figure 8 embodies the functional layers discussed previously. In most instances a sharp demarcation line existed between layers, but in a few cases, compositional gradation was considered in an effort to eliminate this problem. For the most part, the layers were stacked such that CTE values increased as their distances from the substrate increased. However, deviations from this pattern were also made; i.e., the compliant and carbon diffusion layers were interchanged.

Layer components and their stacking order in the overall structure are presented in Table III. An attempt was made to establish a correspondence between the layer designation in Table III and the functional layers designated in Figure 8; this was not possible in all cases. For example, several sample configurations such as specimen 9-44 were processed to assess experimental procedure.

The specimens are categorized by erosion layer (HfO_2 , Y_2O_3 , Al_2O_3 , HfTiO_4 , or Miscellaneous) and they are arranged in order of increasing specimen number. Equilibrium products are listed instead of the starting mixtures. For example, $\text{HfC}+2\text{SiC}+\text{C}$ or H1 is listed instead of HfSi_2+3C . It can be seen that both stabilized and unstabilized forms of HfO_2 were employed. Furthermore, the erosion layer in some instances was applied by plasma spraying; a powder/binder or slurry technique was the alternative method.

Additional specimens are listed in Table IV. These were prepared by a variety of techniques for oxidation testing. It should be recalled that the Table II specimens were fabricated solely for structural examination after fabrication. Attempts were

made to simulate the structural arrangement of Table III specimens in the oxidation specimens by incorporating compliant and barrier layers. Specimens 5-65A-H deviate from the norm in that SiC was chemically vapor deposited over compliant layers of SiC and $\text{TiC}+2\text{SiC}$.

I. Evaluations

The bulk of the inspection effort was done on cross sections cut from fabricated or oxidized specimens. It was difficult to visually assess surface features of hot-pressed specimens because of adhering GRAFOIL™. Metallographically mounted and polished sections were examined optically and by scanning electron microscope (SEM). This effort provided information on layer thicknesses and uniformity, structural integrity in terms of microcrack formation, chemical and physical stability, bonding, etc. Energy dispersive X-rays (EDX) in conjunction with SEM were used to identify elemental constituency of certain phases and elemental diffusion. These analysis were done on majority of Table II and Table IV specimens.

Oxidation tests up to 3000°F (1600°C) were conducted in stagnant air using a CM furnace equipped with MoSi_2 heater elements. The specimens were supported on SiC single crystal chips. After cooling, specimens were removed, weighed and examined for possible failure sites, cracks, etc.

RESULTS AND DISCUSSION

Microstructural Evaluations - The multilayer configurations presented in Tables III, A, B, C, D and E were examined primarily by metallographic methods to ascertain structural integrity. In some instances SEM and EDX complimented the optical work.

The results of these analyses are summarized in Tables V, A, B, C, D and E; a spread sheet format similar to Table III was employed in order to simplify correlations. The crack frequency for each layer roughly corresponds to the vertical line population. Reaction areas and delaminations are also identified. The crack population was derived from an average 100X photomicrograph.

Delaminations are prevalent in compliant layers based on pyrolytic deposits (PGD) and pyrolytic graphite (PG). The specific compliant layers which failed can be identified in the various Table V's. The nature of PGD failures can be seen in Figures 9 and 10; PG failures were similar.

Similarly, delaminations frequently are observed in CC substrates having a compliant layer stacked with one or more layers. Compliant layers derived by equation (1) reaction process rarely failed in the PG or PGD modes. A solitary compliant layer has little effect on CC structural integrity (see Figure 12). Typical CC failures are presented in the photomicrographs of Figures 11, 17 and 23. Failures in 11 and 23 can be attributed to poor CC shear strength and the interfacial failure in Figure 17 is a result of poor bond strength between the compliant layer and CC. A thin PG coating on the CC surface has an adverse effect on reactivity and bonding. It has been observed this layer restricts internal penetration of the reactive melt.

An example of a pitch-graphite compliant layer is shown in Figure 8. This system has performed without developing flaws and has potential except for processing time to achieve suitable layer thickness.

According to the data in Tables V, the outer HfO_2 layer has less tendency to crack than Y_2O_3 . There is insufficient data to make comparisons with the other oxide layers. The principal objection to cracked outer ceramics is their reduced effectiveness as oxygen diffusion barriers.

Crack information such as origin, propagation distance and direction was extracted from photomicrographs of multilayer specimens presented in Figures 10-22. The cracks considered in this exercise are those which transverse the multilayers in a direction normal to the substrate. This data is represented as vectors in Table VII. It is possible in an empirical way to correlate the vector features with disposition of the layers, with due consideration given to their CTE values and in placement of the compliant layer.

Table VII

Cracking Behavior in Multilayer Configurations

Spec No.	Figure No.	Multilayer Configuration
4-92	11	$\overrightarrow{\text{HfO}_2/\text{H1}/\text{CC}}$
8-27	17	$\overrightarrow{\text{HfO}_2/\text{AlN}/\text{H0}/\text{H5}/\text{CC}}$
2-42	19	$\overrightarrow{\text{Y}_2\text{O}_3/\text{H1}/\text{Pitch} + \text{Graphite}/\text{ATJ}}$
2-96	20	$\overrightarrow{\text{Y}_2\text{O}_3/\text{TaC}/\text{H0}/\text{Pitch} + \text{Graphite}/\text{ATJ}}$
7-100	22	$\overleftarrow{\text{Y}_2\text{O}_3} + \overleftarrow{\text{HfO}_2/\text{Y}_2\text{O}_3} + \overleftarrow{\text{HfC}/\text{SiC}} + \overleftarrow{\text{HfC}/\text{H0}/\text{ATJ}}$
2-38	10	$\overleftrightarrow{\text{HfO}_2/\text{TiN}/\text{H0}/\text{PGD}/\text{ATJ}}$
3-63	14	$\overleftarrow{\text{HfO}_2/\text{T0}/\text{TaC}/\text{Pitch} + \text{Graphite}/\text{ATJ}}$
10-38	15	$\overleftarrow{\text{HfO}_2/\text{SiC}/\text{H0}/\text{TaC}/\text{ATJ}}$
2-100	13	$\overleftarrow{\text{HfO}_2/\text{H2}/\text{TaC}/\text{ATJ}}$

According to data in Table VII, compliant layers do not prevent cracks from forming. This is very apparent in those

specimens having the compliant layer positioned near the substrate (see Figures 11, 17, 19 and 20). The cracks develop in the tensile stressed oxygen barrier or erosion layers and they propagate inward. Most cracks are arrested at low CTE compressively loaded layers such as AlN or the compliant ones. The shear cracks frequently seen in AlN might be a consequence of this type loading.

It is possible to manipulate the crack origin as was done for specimens 2-100, 3-63 and 10-38. Crack vector changes for this series of specimens are evident in Figures 13, 14 and 15, respectively. High CTE TaC positioned adjacent to low CTE ATJ becomes tension loaded during cool down and, accordingly, is the origin of cracks in these specimens. Cracks propagated away from the substrate, but are effectively arrested by compliant layers with free graphite (see Specimen 2-100, Figure 13).

Cracks can also be initiated at the subsurface locations by appropriately adjusting CTE relationships. Excellent examples of this phenomenon are apparent in Figures 10 and 22.

The multilayer structure in Figure 21 was compositionally tailored to provide a CTE gradation from Y_2O_3 to ATJ. Although a sharp compositional transition is apparent between Y_2O_3 and Y_2O_3+TaC , it can be seen the crack does not originate there, but at the Y_2O_3 surface. The TaC particles appear to interact with the crack and retard its progress. Similar structural features are apparent in Figure 16 for specimen 7-12. The very few cracks in this specimen originated at the HfO_2 surface.

The coating systems in Figures 21 and 22 are quite similar except for an interchange between HfO_2 , and Y_2O_3 . Microstructural features and cracking patterns, however, are strikingly different. Similarly, analytical work established differences in phase constituency and conceivably CTE. These results clearly illustrate

the importance of thermochemical considerations in the design of multilayer coatings.

Specimen #8-87 was processed to the point of being virtually crack free. The layering sequence was as follows:

HfO_2 + 15 w/o SiC whiskers/AlN/SiC/H5/CC.

This system is unique in that the erosion layer consisted initially of SiC whiskers and HfO_2 . The photomicrograph in Figure 18 shows the coating and unusual erosion layer. A similar layered structure without SiC whiskers typically would develop a network of cracks extending from the HfO_2 surface to AlN. X-ray analysis of a HfO_2 + 15 w/o SiC whisker compact processed to 3360°F (1850°C) for one hour revealed only HfC.

Compliant Layer Properties - Test bars of the compliant composite $\text{HfC}+2\text{SiC}+\text{XC}$ were prepared by hot pressing mixtures of HfSi_2 and graphite powder at 1850°C. The data in Table VII for these specimens includes percent theoretical density, Young's modulus and thermal expansion coefficient for the 70°-1470°F (25°-800°C) temperature range. Major increases in free graphite do not affect densification significantly; however, Young's modulus is appreciably reduced and compliancy is increased. The CTE is low for a specimen with $\text{X}=0$; remaining values are approximately equivalent to SiC.

Table VIII

Properties of HfC + 2SiC + XC, A Compliant Composite

X	% Theoretical Density	E ($\times 10^6$ psi)	σ ($\times 10^{-6}$ °C ⁻¹)
0	72.7	23.7	6.2
2	68.0	12.1	4.0
4	64.1	7.1	5.3
6	65.6	6.3	5.2

Oxidation Results - The oxidation results in Table VI are for specimen coatings fabricated by: (1) chemical vapor deposition; (2) reactive sintering; (3) quasi-isostatic hot pressing; and (4) hot pressing. The fabrication method had a significant effect on coating density, overall coating integrity and ultimately oxidation protection.

A limited amount of CVD work was performed. The effort was restricted to assessing the effect of a compliant layer on crack formation in the coating. CVD SiC has a higher CTE than ATJ graphite or CC; this ultimately culminates in a microcracked coating. Photographs of three oxidized CVD coated specimens are shown in Figure 24. They were oxidized at 2375°F (1300°C) for approximately 100 hours. Specimen (A) did not have a compliant layer; specimens (B) and (C) had compliant layers in the form of porous SiC and SiC + TiC, respectively. Microcracking is very prevalent and obvious in photograph (A), but cracks are very sparse in specimen photos designated as (B) and (C). Oxidation results presented in Table VI relate very well to the frequency of microcracks. The compliant layer on specimen (C) and the corresponding oxidized specimen are shown in Figure 25. The porous nature of the compliant layer is partially retained in the CVD

coated specimen. Attempts to fabricate crack-free CVD coatings on CC with the above compliant layer process were unsuccessful.

Reasonably good oxidation results were obtained for reaction sintered coatings in the temperature range 1880°-2550°F (1000°-1400°C). For example, Specimens 6-49 (A) and 6-49 (B) were oxidized for 300 hours at 1880°F (1000°C) with losses as low as 0.19%; Specimen #11-14B was oxidized at 2550°F (1400°C) for 38 hours and lost 4.88%. Short duration runs to 3000°F (1600°C) were also successful. Oxidized products in these specimens typically include Al_2O_3 , SiO_2 , and TiO_2 . This oxide mixture forms a fluid melt at approximately 2550°F (1400°C) according to Agaman and White.⁽¹⁰⁾ The semi-porous plasma sprayed erosion layers permit oxygen ingress for ultimate conversion of the refractories to oxides.

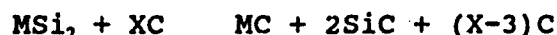
The coatings prepared by quasi-isostatic hot pressing were not uniformly densified; a condition which adversely affected oxidation protection results. Specimens such as 10-35 (A) and (B), 10-51, 10-56, 11-37 and 11-38 are a series with coatings densified by this process. The oxidation results shown for this series in Table VI are similar in that rapid deterioration occurred within one hour at 2550°F (1400°C).

Coatings on surfaces perpendicular to press rams are easily densified by hot pressing. Slightly curved surfaces are also manageable, but coated perimeter areas parallel to the ram are incapable of being densified. Thus, hot pressed coatings were not prepared for oxidation testing. A number of one-inch diameter pellets were prepared from refractory substances for evaluation. These included AlN (#'s 10-14 (a) (b) (c)); a potentially valuable crack-stopper. Tests at 2550°F (1400°C) revealed excessive oxidation had occurred before 42 hours (see Table VI). Other

refractory mixtures densified for testing included $\text{HfB}_2 + \text{SiC}$ (#10-15 (a) (b)), AlN-SiC-BN (#10-17), $\text{MoSi}_2 + \text{Al}_2\text{O}_3$ (#11-18), $\text{Y}_2\text{O}_3 + \text{MoSi}_2$ (#11-29), $\text{HfB}_2 + \text{Al}_2\text{O}_3$ (#12-38). Satisfactory oxidation results are shown in Table VI for these blends. The $\text{MoSi}_2 + \text{Al}_2\text{O}_3$ blend subsequently functioned well as an oxygen diffusion barrier in conjunction with a reaction sintered system.

CONCLUSIONS

An effective compliant layer employed in multilayer configurations was synthesized by hot pressing an appropriate disilicide/graphite blend. Free graphite which imparts compliancy coexists with the reaction products MC and SiC when X exceeds 3 in the following expression:



The Young's modulus, a corollary to compliancy, decreased from 23.7×10^6 psi for $\text{X}=3$ to 7.1×10^6 psi for $\text{X}=7$.

The above chemical concept can be used to formulate compliant layers for use in CVD SiC systems and for reaction sintered multilayered coatings. These compliant structures preferably are porous and carbon-free.

After examining the microstructures of numerous as fabricated multilayer configurations, it became apparent that crack initiation and propagation can be controlled to a degree greater than previously expected. For example, a CTE graded configuration ranging from high at the surface toward low at the substrate invariably developed cracks at the tensile loaded high CTE surface and the cracks propagate toward the substrate. If the gradation is interrupted by a low CTE intermediate layer, cracks initiated at

the surface terminate at the low CTE component. The low CTE layer undoubtedly is loaded in compression. A high CTE layer positioned between the substrate and a graphite loaded compliant layer has practical implications because cracks initiated in the high CTE layer propagate into the compliant layer and are arrested. Graphite particles in the compliant layer effectively blunt the crack propagation. The coating surface remains crack-free which is important for reducing oxygen transport to the coating interior and substrate. The above concept could contribute to processing crack free CVD SiC or Si_3N_4 .

One of the few specimens fabricated without apparent cracking had the following configuration:

HfO_2 + 15 w/o SiC whiskers/AlN/SiC/H5/CC

It was confirmed, however, the composite surface layer was converted to HfC. The effect this conversion had on the coating stress states is not clear at this time.

Crack-free CVD SiC coatings were produced on ATJ Grade graphite featuring compliant layers. Oxidation results were excellent for this series of specimens.

Reaction sintered coatings involving disilicide and graded amounts of Al_2O_3 provided reasonable protection to 2550°F (1400°C). This operational temperature is limited by fluid melts formed from TiO_2 , SiO_2 , Al_2O_3 oxide products. The concept has merit providing higher melting oxide systems are created.

Hot pressed coatings generally are too porous and incapable of providing adequate oxidation protection.

SUMMARY AND RECOMMENDATIONS

Based on the fabrication and examination of numerous multilayer microstructures, an empirical concept was developed for producing oxygen barrier layers with a minimum number of flaws.

Crack initiation and propagation can be controlled by giving judicious consideration to placement of the layers. In this regard, layer CTE and compliance are of great importance. Cracks will develop in high CTE or tensile loaded layers and they will propagate until halted by low CTE or compressively loaded layers. A compliant layer with free graphite is an effective crack stopper.

An effective compliant layer was produced by reacting a disilicide and graphite mixture. This blend was stacked along with the layered powders during pressing. Thus, a ternary mixture of $2\text{SiC} + \text{MC} + \text{XC}$ was produced in-situ while densifying the layered powders.

Best oxidation protection was provided by CVD SiC applied on ATJ graphite coated with compliant layers of SiC and SiC + TiC. This approach was effective with monolithic graphite substrate, but not with CC. However, a layered system with appropriate positioning of constituents such that cracks propagate away from CC should render crack-free SiC coatings.

Moderately good oxidation protection was achieved with reaction sintered coatings. The present limiting operational temperature of 2250°F (1400°C) was attributed to fluid ternary oxide melts.

Accordingly, multilayer coatings are capable of providing effective protection to CC composites. Since crack-free coatings are difficult to achieve, future work should expand on the concept presented here where consideration was given to manipulating the crack origin, its propagation direction and stoppage mechanisms. Finally, emphasis should be placed on CVD coatings because they are very dense, generally impervious and, therefore, highly suitable as diffusion barriers.

REFERENCES

1. Ehrburger, P., "Protective Layers for Special Types of Composites," Carbon Fibers Filaments and Composites, 1990, Kluwer Academic Publishers, printed in Netherlands, J. L. Figueiredo, et al. (eds.), 327-336.
2. Strife, J. R., J. E. Sheehan, "Ceramic Coatings for Carbon-Carbon Composites," Ceramic Bull. 67 [2] 369-374 (1988).
3. Criscione, J. M., R. A. Mercuri, E. P. Schram, A. W. Smith, H. F. Volk, "High Temperature Protective Coatings for Graphite," ML-TDR-64-173, 1964.
4. Glatter, I. Y., D. J. Treacy, J. E. Sheehan, K. S. Mazdiasni, "High Temperature Chemical Behavior of a Mulci-Layered Oxidation Protection Coating System for Carbon-Carbon Composites," WRDC-TR-89-4127, 1989.
5. Sara, R. V., "Carbonaceous Articles Having Oxidation Prohibitive Coatings Thereon," U. S. Patent 4,567,103, January, 1986.
6. Strife, J. R., "Development of High Temperature Oxidation Protection for Carbon-Carbon Composites," Report No. NADC-86087-60, April, 1985.
7. Sheehan, J. E., "Oxidation Protection for Carbon Fiber Composites," Carbon 27 [5] 709-715 (1989).
8. Electroconsolidation™ Basic Industrial Research Laboratory, Northwestern University, Evanston, Illinois.
9. Smurov, I., A. Uglov, Yu. Krivonogov., "Pulsed Laser Treatment of Plasma-Sprayed Thermal Barrier Coatings: Effect of Pulse Duration and Energy Input," Jour. Mat. Sci. 27 (1992) 4523-4530.
10. Agamawi, Y. M., J. White, Trans. Brit. Ceram. Soc. 51, 319 (1951-52).

APPENDIX

Table II
Powder Materials and Their Characteristics

Material	Source	Grade	Purity	Particle Size
AlN	Tokuyama	F	Ultra High	<1 μ m
Al ₂ O ₃	Alcoa	T-61	High	-325 Mesh
Al ₂ O ₃	Praxair	LA 2-400	High	-200 Mesh
3 Al ₂ O ₃ • 2 SiO ₂	Washington Mills Electro Minerals Corp.	Grit Size	----	-100 Mesh
B	ALFA		97.0%	1 - 10 μ m
B ₂ C	ALFA	-----	77.54% B	-325 Mesh
CrB ₂	Cerac	-----	99.5%	-325 Mesh
Graphite Powder	UCAR Carbon	GP-39	High	-44 μ m
HfB ₂	Cerac	-----	99.5%	-325 Mesh
HfC	Cerac	-----	99.5%	-325 Mesh
HfO ₂	Cerac	-----	99.5%	
HfO ₂ 5-10 w/o Y ₂ O ₃	Cerac	-----	99.0%	-150 + 325 Mesh
HfSi ₂	Cerac	-----	99.5%	-100 Mesh
HfTiO ₄	Cerac	-----	99.5%	-325 Mesh
La ₂ O ₃	John Matthey	-----	99.99%	
MoSi ₂	Union Carbide	-----	----	-325 Mesh
Si	ALFA	-----	High	-325 Mesh
β -SiC	Hermann Starck	B10	97.5%	-5 μ m
SiC	Carborundum	-----	----	-280 Mesh
β -SiC	Superior Graphite	059	~97.5%	-2 μ m
SiO	Cerac	-----	99.9%	-325 Mesh
SiO ₂	ALFA	-----	99.5%	-325 Mesh
Si ₃ N ₄	ALFA	-----	99.5%	-325 Mesh
Si ₃ N ₄	Toya Soda	TS 8	98.5%	<1 μ m
TaB ₂	Hermann Starck	-----	----	-325 Mesh
TaC	Cerac	-----	99.5%	-325 Mesh
TaN	Cerac	-----	99.5%	-325 Mesh
TaSi ₂	Cerac	-----	99.5%	-325 Mesh
TiN	Cerac	-----	99.5%	-325 Mesh

Table II
Powder Materials and Their Characteristics
(Continued)

Material	Source	Grade	Purity	Particle Size
TiSi ₂	Hermann Starck	-----	99.4%	-325 Mesh
WC	Cerac	-----	99.5%	-1 μ m
Y ₂ O ₃	Cerac	-----	99.9%	-150 + 325 Mesh
Y ₃ Al ₅ O ₁₂ (YAG)	Cerac	-----	99.9%	-1/2" + 1/8"
ZrB ₂	Cerac	-----	99.5%	-325 Mesh
ZrB ₂	Norton	-----	-----	-325 Mesh
ZrC	Cerac	-----	99.5%	-325
ZrO ₂ - 3 Y ₂ O ₃	Toya Soda	TZ-34	99.3%	<1 μ m
ZrO ₂ - 8 Y ₂ O ₃	Praxair	ZRO-156	High	-----
ZrO ₂	Zircar	-----	-----	-10 μ m

Table IIIA

Multilayer Configurations and Stacking Arrangement

Spec. No.	LAYER				
	1	2	3	4	5
1-93	HfO ₂	AlN	TaC	PGD ⁽³⁾	ATJ
1-94	HfO ₂	TaB ₂	TaC	PGD	ATJ
1-99 (a)	HfO ₂	AlN	TaB ₂	Pitch + Graphite	ATJ
2-17 (a)	HfO ₂	AlN	TaC	PG ⁽⁴⁾	---
2-18 (b)	HfO ₂	AlN	TaC	PGD	ATJ
2-19	HfO ₂		TaC	PGD	ATJ
2-20	HfO ₂		HO ⁽¹⁾	PGD	ATJ
2-22	HfO ₂	AlN	HO	PGD	ATJ
2-38	HfO ₂	TiN	HO	PGD	ATJ
2-39 (c)	HfO ₂	AlN	TaC	PG	---
2-40 (b)	HfO ₂	AlN	TaB ₂	Pitch + Graphite	ATJ
2-43	HfO ₂		H1	PGD	ATJ
2-85	HfO ₂	HfB ₂	HO	Pitch + Graphite	ATJ
2-100	HfO ₂		H2	TaC	ATJ
3-63	HfO ₂	T0	TaC	Pitch + Graphite	ATJ
3-98	HfO ₂			HO	CC
3-100	HfO ₂		TaC	T0	CC
4-39	HfO ₂	AlN	T0	T0.47C	CC
4-92(a) (b) (c)	HfO ₂			H1	CC
7-12	HfO ₂	HfC + HfO ₂	HfC, HfC + SiC	HO	ATJ
7-52 (B)	HfO ₂ ⁽²⁾	TiSi ₂ + 3 w/o CrB ₂	TiSi ₂ + 3 w/o CrB ₂	TiSi ₂ + 3 w/o CrB ₂	ATJ
7-100 (A)	HfO ₂ + Y ₂ O ₃	Y ₂ O ₃ + HfC	HfC + SiC	HO	ATJ
7-100 (B)	HfO ₂	AlN	T0	T0.47	ATJ
8-19 (A)	HfO ₂ + 15 w/o SiC Whiskers	HfO ₂ + 3HfC	HfC + SiC	HO	ATJ
8-19 (B)	HfO ₂	HfC + 15 w/o SiC Whiskers	HfC + SiC	HO	ATJ
8-27	HfO ₂	AlN	HO	H5	CC
8-82	HfO ₂	AlN	SiC	H2, H5	CC
8-83 (A) (a)	HfO ₂	AlN	SiC	H2	CC

Table IIIA
Multilayer Configurations and Stacking Arrangement
(Continued)

Spec. No.	LAYER				
	1	2	3	4	5
8-83 (B) (a)	HfO ₂	AlN	SiC	H4	CC
8-85	HfO ₂	AlN	SiC	H2, H5	CC
8-87	HfO ₂ + 15 w/o SiC Whiskers	AlN	SiC	H5	CC
9-67 (b)	HfO ₂	AlN	SiC	H4	CC
9-74	HfO ₂		HO	TaC	CC
10-12	HfO ₂	HfB ₂ + SiC		H4	CC
10-37 (A) (b)	HfO ₂	AlN	SiC	H2	CC
10-37 (B) (c)	HfO ₂	AlN	SiC	H4	CC
10-38	HfO ₂	SiC	HO	TaC	ATJ

Table IIIB
Multilayer Configurations and Stacking Arrangement

Spec. No.	LAYER				
	1	2	3	4	5
1-64	Y_2O_3	AlN	SiC		ATJ
1-66	Y_2O_3	TaB ₂	TaC		PG
1-67	Y_2O_3	TaSi ₂	TiC		PG
1-74	Y_2O_3	HfSi ₂	TaC		PG
1-84	Y_2O_3	AlN	TaSi ₂		PG
1-85	Y_2O_3		TaC		PG
1-86	Y_2O_3	AlN		H0	PG
1-87 (a)	Y_2O_3	AlN	TaC		PG
1-88	Y_2O_3	TaSi ₂	TaC		PG
1-96 (b)	Y_2O_3	AlN	TaC		PG
1-98	Y_2O_3	AlN	TaB ₂		PG
2-42	Y_2O_3			H1, Pitch + Graphite	ATJ
2-96	Y_2O_3		TaC	H0, Pitch + Graphite	ATJ
3-99	Y_2O_3			HTO, T0	CC
7-4	Y_2O_3	Y_2O_3 + TaC	SiC + TaC	H0	ATJ
7-21	Y_2O_3	Y_2O_3 + 3HfC	SiC + HfC	H0	ATJ
7-48	Y_2O_3	5 Y_2O_3 + 2HfC	Y_2O_3 + HfC	SiC + HfC, H0	ATJ
7-52	Y_2O_3	TiSi ₂ + 3 w/o CrB ₂	TiSi ₂ + 3 w/o CrB ₂	TiSi ₂ + 3 w/o CrB ₂	ATJ
7-99 (A)	Y_2O_3 + 15 w/o SiC Whiskers	Y_2O_3 + 3HfC	SiC + HfC	H0	ATJ
7-99 (B)	Y_2O_3 + HfC		SiC + HfC	H1	ATJ
7-100	Y_2O_3 + HfO ₂	Y_2O_3 + HfC	SiC + HfC	H0	ATJ
10-12	Y_2O_3	HfB ₂ + SiC		H4	CC
10-53	Y_2O_3	60 v/o Y_2O_3 + 40 v/o TaC	25 v/o Y_2O_3 + 75 v/o TaC	H0, H2	ATJ

Table IIIC

Multilayer Configurations and Stacking Arrangement

Spec. No.	LAYER				
	1	2	3	4	5
6-49 (B)	Al_2O_3	$\text{TiSi}_2 + 15 \text{ w/o } \text{Al}_2\text{O}_3$	$\text{TiSi}_2 + 3 \text{ w/o } \text{CrB}_2$		ATJ
9-29	Al_2O_3		SiC	H4	CC
9-68 (a)	Al_2O_3	AlN	SiC	H4	CC
9-72 (b)	Al_2O_3	AlN	SiC	H4	CC

Table IIID

Multilayer Configurations and Stacking Arrangement

Spec. No.	LAYER				
	1	2	3	4	5
2-92	$\text{ZrO}_2 \cdot \text{S}$		HO	PGD	ATJ
2-94	$\text{ZrO}_2 \cdot \text{S}$		HO	Pitch - Graphite	ATJ
2-95	$\text{ZrO}_2 \cdot \text{S}$	TiN	HO	PGD	ATJ
2-99	$\text{ZrO}_2 \cdot \text{S}$		TaC	Pitch - Graphite	ATJ

Table IIIE

Multilayer Configurations and Stacking Arrangement

Spec. No.	LAYER				
	1	2	3	4	5
4-64 (a) (b) (c)	HfTiO_4			HO	CC
4-65 (a) (b) (c)	HfTiO_4			$0.33 \text{ HfSi}_2 + 0.67 \text{ HO}$	CC
4-76 (a) (b) (c)	HfTiO_4			$0.67 \text{ HfSi}_2 + 0.33 \text{ HO}$	CC

Table IIIF
Multilayer Configurations and Stacking Arrangement

Spec. No.	LAYER				
	1	2	3	4	5
5-61 (A)	TiSi ₂ + 5 w/o CrB ₂			H5	CC
6-74	TiSi ₂ + 25 w/o Al ₂ O ₃	TiSi ₂ + 3 w/o CrB ₂			ATJ
8-22 (A)	SiC			Ti2, 0.67 TiO + 0.33 TiSi ₂	3DCC
8-22 (B)	SiC			Ti3, Ti5	3DCC
8-36 (A)	SiC			Ti2, Ti7	3DCC
8-36 (B)	SiC			Ti3, Ti9	
8-84	YAG	AlN	SiC	H2, H5	
9-27				H5	CC
9-28 (a)	89.5 w/o Si ₃ N ₄ + (5.5 w/o Al ₂ O ₃ + 5.0 w/o Y ₂ O ₃)		SiC	H4	CC
9-30 (b)	89.5 w/o Si ₃ N ₄ + (5.5 w/o Al ₂ O ₃ + 5.0 w/o Y ₂ O ₃)		SiC	H4	CC
9-31 (a)	SiC			H4	CC
9-43				H2	CC
9-44 (a,b,c, d,e,f)				H4	CC
9-66 (b)	SiC			H4	CC
9-71				H7	CC
11-36	La ₂ O ₃ · 2ZrO ₂	HfB ₂ + SiC		H2	ATJ

- (1) H0 = HfC + 2SiC
H1 = HfC + 2SiC + C
H2 = HfC + 2SiC + 2C
H3 = HfC + 2SiC + 3C
Etc.

H = HfC
T = TaC
Ti = TiC

- (2) S = Stabilized

- (3) Pyrolytic graphite deposit (40 μm on ATJ)
Pyrolytic graphite (1/8" thick)

- (4) Compositions are in moles except where noted.

a, b, etc. - Same formulation, different processing.

Table IV
Oxidation Specimens

Spec. No.	LAYER				
	1	2	3	4	5
5-65 (A)	SiC			TiSi ₂ + 2 w/o C	ATJ
5-65 (B)	SiC			TiSi ₂ + 5 w/o C	ATJ
5-65 (C)	SiC			TiSi ₂ + 3 w/o C	ATJ
5-65 (D)	SiC			TiSi ₂ + 4 w/o C	ATJ
5-65 (E)	SiC			Si	ATJ
5-65 (F)	SiC			TiSi ₂ + 5 w/o CrB ₂	ATJ
5-65 (G)	SiC			TiSi ₂	ATJ
5-65 (H)	SiC				ATJ
6-49 (A)	Al ₂ O ₃	TiSi ₂ + 25 w/o Al ₂ O ₃	TiSi ₂ + 10 w/o Al ₂ O ₃	TiSi ₂ + 3 w/o CrB ₂	ATJ
6-49 (B)	Al ₂ O ₃	TiSi ₂ + 15 w/o Al ₂ O ₃	TiSi ₂ + 3 w/o CrB ₂		ATJ
6-78	Al ₂ O ₃	TiSi ₂ , TiSi ₂ + 25 w/o Al ₂ O ₃	TiSi ₂ + 10 w/o Al ₂ O ₃	TiSi ₂ + 3 w/o B ₄ C	ATJ
7-1	Al ₂ O ₃	ZrSi ₂ + 15 w/o Al ₂ O ₃	ZrSi ₂ + 3 w/o ZrB ₂	SiC + B ₄ C	ATJ
7-7 (B)	Al ₂ O ₃	TiSi ₂ + 25 w/o Al ₂ O ₃	TiSi ₂ + 10 w/o Al ₂ O ₃	SiC + B ₄ C	ATJ
7-9	Al ₂ O ₃	TiSi ₂ , TiSi ₂ + 25 w/o Al ₂ O ₃	TiSi ₂ + 10 w/o Al ₂ O ₃	TiSi ₂ + 3 w/o B ₄ C	ATJ
7-49 (A)	Y ₂ O ₃	TiSi ₂ + 3 w/o CrB ₂	TiSi ₂ + 3 w/o CrB ₂	TiSi ₂ + 3 w/o CrB ₂	ATJ
7-49 (B)	HfO ₂	TiSi ₂ + 3 w/o CrB ₂	TiSi ₂ + 3 w/o CrB ₂	TiSi ₂ + 3 w/o CrB ₂	ATJ
7-58 (A)	HfO ₂	TiSi ₂ + 3 w/o CrB ₂	TiSi ₂ + 3 w/o CrB ₂	TiSi ₂ + 3 w/o CrB ₂	ATJ
7-58 (B)	Y ₂ O ₃	TiSi ₂ + 3 w/o CrB ₂	TiSi ₂ + 3 w/o CrB ₂	TiSi ₂ + 3 w/o CrB ₂	ATJ
7-75 (A)	HfO ₂ (S)	TiSi ₂ + 3 w/o CrB ₂	TiSi ₂ + 3 w/o CrB ₂	TiSi ₂ + 3 w/o CrB ₂	ATJ
7-75 (B)	Y ₂ O ₃	TiSi ₂ + 3 w/o CrB ₂	TiSi ₂ + 3 w/o CrB ₂	TiSi ₂ + 3 w/o CrB ₂	ATJ
7-82 (A)	SiC			TiSi ₂ + 4 w/o C	CC
7-82 (B)	SiC			TiSi ₂ + 6 w/o C	CC
10-14 (a,b,c)	AlN				
10-15	30 v/o HfB ₂ + 70 v/o SiC				

Table IV
Oxidation Specimens
(Continued)

Spec. No.	LAYER				
	1	2	3	4	5
10-17	65.9 v/o AlN + 20.8 v/o SiC + 13.4 v/o BN				
10-45 (A)	HfO ₂ + 15 w/o SiC Whiskers	3 HfC + HfO ₂	HfC + SiC	H0	CC
10-45 (B)	HfO ₂ + 15 w/o SiC Whiskers	3 HfC + HfO ₂	HfC + SiC	H2	CC
10-51	HfO ₂	AlN	Ti2	TaC	ATJ
10-56	30 v/o HfB ₂ + 70 v/o SiC			H2	ATJ
11-9	Al ₂ O ₃	TiSi ₂ + 25 w/o Al ₂ O ₃	TiSi ₂ + 10 w/o Al ₂ O ₃	TiSi ₂	ATJ
11-13	70 v/o MoSi ₂ + 30 v/o HfB ₂				
11-14 (A)	MoSi ₂	TiSi ₂ + 25 w/o Al ₂ O ₃	TiSi ₂ + 10 w/o Al ₂ O ₃	TiSi ₂	ATJ
11-14 (B)	38 v/o MoSi ₂ + 62 v/o Al ₂ O ₃	TiSi ₂ + 25 w/o Al ₂ O ₃	TiSi ₂ + 10 w/o Al ₂ O ₃	TiSi ₂	ATJ
11-16 (B)	Al ₂ O ₃	TiSi ₂ + 25 w/o Al ₂ O ₃	TiSi ₂ + 10 w/o Al ₂ O ₃	TiSi ₂	ATJ
11-18	38 v/o MoSi ₂ + 62 v/o Al ₂ O ₃				
11-29	56 v/o Y ₂ O ₃ + 44 v/o MoSi ₂				
11-37	30 v/o HfB ₂ + 70 v/o SiC			H4	ATJ
11-38	60 v/o Y ₂ O ₃ + 40 v/o SiC	25 v/o Y ₂ O ₃ + 75 v/o SiC	H0	H2	ATJ
11-54 (Cube)	30 v/o HfB ₂ + 70 v/o SiC		SiC	H4	ATJ
11-90 (Cube)	30 v/o HfB ₂ + 70 v/o SiC	SiC	H4	TaC	ATJ
11-91 (Cube)	30 v/o HfB ₂ + 70 v/o SiC	SiC	H4	HfSi ₂	ATJ
11-92 (Cube)	30 v/o HfB ₂ + 70 v/o SiC	SiC	H0	TaC	ATJ
11-88 (A)	ZrO ₂	HfSi ₂ + 25 w/o Al ₂ O ₃	HfSi ₂ + 10 w/o Al ₂ O ₃	HfSi ₂	ATJ

Table IV
Oxidation Specimens
(Continued)

Spec. No.	LAYER				
	1	2	3	4	5
11-88 (B)	38 v/o MoSi ₂ + 62 v/o Al ₂ O ₃	HfSi ₂ + 25 w/o Al ₂ O ₃	HfSi ₂ + 10 w/o Al ₂ O ₃	HfSi ₂	ATJ
11-30 (A)	ZrO ₂	TiSi + 25 w/o Al ₂ O ₃	TiSi ₂ + 10 w/o Al ₂ O ₃	TiSi ₂	ATJ
11-30 (B)		TiSi ₂ + 25 w/o Al ₂ O ₃	TiSi ₂ + 10 w/o Al ₂ O ₃	TiSi ₂	ATJ
12-38	26 v/o HfB ₂ + 74 v/o Al ₂ O ₃				
12-39	26 v/o HfB ₂ + 74 v/o Al ₂ O ₃ ,	TiSi ₂ + 25 w/o Al ₂ O ₃	TiSi ₂ + 10 w/o Al ₂ O ₃	TiSi ₂	ATJ
	38 v/o MoSi ₂ + 62 v/o Al ₂ O ₃				

Table VA

Summary of Microstructural Assessment of As-Processed Specimens

Spec. No.	LAYER				
	1	2	3	4	5
1-93					d ATJ
1-94					d ATJ
1-99 (a)		R	d		ATJ
2-17 (a)					ATJ
2-18 (b)		R			d ---
2-19					d ATJ
2-20		R			dR ATJ
2-22		R			dR ATJ
2-38	R		R	d	d ATJ
2-39 (c)					dR ---
2-40 (b)					ATJ
2-43	R		R		d ATJ
2-85	R				ATJ
2-100	R				ATJ
3-63	R				R ATJ
3-98					dR CC
3-100	R				d CC
4-39	R			R	d CC
4-92(a) (b) (c)					CC
7-12					ATJ
7-52 (B)					ATJ
7-100 (A)					ATJ
7-100 (B)					ATJ
8-19 (A)					ATJ
8-19 (B)	R				ATJ
8-27	R				d CC
8-82	R		R		CC
8-83 (A) (e)					d CC

Table VA
Summary of Microstructural Assessment of As-Processed Specimens
(Continued)

Spec. No.	LAYER									
	1	2	3	4	5					
8-83 (B) (a)									d	CC
8-85									d	CC
8-87										CC
9-67 (b)	R								d	CC
9-74	R									CC
10-12									d	CC
10-37 (A) (b)									d	CC
10-37 (B) (c)	R		R							CC
10-38	R		R							ATJ

Table VB

Summary of Microstructural Assessment of As-Processed Specimens

[illegible]

Table VC

Summary of Microstructural Assessment of As-Processed Specimens


Spec. No.	LAYER				
	1	2	3	4	5
6-49 (B)					ATJ
9-29					CC
9-68 (a)					d CC
9-72 (b)		R			d CC

Table VD

Summary of Microstructural Assessment of As-Processed Specimens

Spec. No.	LAYER				
	1	2	3	4	5
2-92	R		R		ATJ
2-94					d ATJ
2-95					ATJ
2-99					ATJ

Table VE

Summary of Microstructural Assessment of As-Processed Specimens

Spec. No.	LAYER				
	1	2	3	4	5
4-64 (a)				d	CC
(b)	R			R	
(c)	R			d	
4-65 (a)	R			R	CC
(b)					
(c)				R	
4-76 (a)	R			R	CC
(b)	R				
(c)					

Table VF

Summary of Microstructural Assessment of As-Processed Specimens

Spec. No.	LAYER				
	1	2	3	4	5
5-61 (A)				d	CC
6-74					ATJ
8-22 (A)					3DCC
8-22 (B)					3DCC
8-36 (A)					3DCC
8-36 (B)					3DCC
8-84					d CC
9-27					CC
9-28 (a)					CC
9-30 (b)					CC
9-31 (a)					CC
9-43					CC
9-44 (a,b,c, d,e,f)					CC
9-66 (b)				d	CC
9-71					CC
11-36				R	ATJ

Vertical lines noted in each layer represent the population of cracks observed in a random 100X photomicrograph.

d = Delamination

R = Reaction

Table VI

Oxidation Test Results

Spec. No.	Oxidation Temperature		Total Time (Hours)	% Weight Change	Remarks
	°F	°C			
5-65 (D)	2375	(1300)	137	+0.05	Very few microcracks
5-65 (E)	2375	(1300)	95	+0.15	Very few microcracks
5-65 (G)	2375	(1300)	92	-2.16	Many microcracks
5-65 (H)	2375	(1300)	95	-2.37	Many microcracks
6-49 (A)	1830	(1000)	300	-0.19	Microcracks noted after 23 hours but they healed
6-49 (B)	1830	(1000)	300	-2.60	
6-78	930	(500)	90	-19.78	-----
7-1	3000	(1600)	2	-----	Deteriorated
7-7 (B)	3000	(1600)	1.5	-7.31	Fused
7-9	3000	(1600)	0.5	-5.79	Fused
7-49 (A) (B)	2550	(1400)	16	-54.77	Fused, cracks
7-58 (A) (B)	2550	(1400)	33	-16.03	HfO ₂ surface good; Y ₂ O ₃ surface badly cracked
7-75 (A) (B)	2730	(1500)	5	-----	HfO ₂ surface rough; Y ₂ O ₃ surface badly flawed
7-82 (A) (B)	-----	-----	--	-----	Flawed, no test
10-14 (a)	2550	(1400)	3	-----	320 μ m - Oxide layer
10-14 (b)	2550	(1400)	21	-----	475 μ m - Oxide layer
10-14 (c)	2550	(1400)	42	-----	1150 μ m - Oxide layer
10-15 (a)	2550	(1400)	38	+0.58	Glazed appearance
10-15 (b)	2550	(1400)	38	+0.87	Glazed appearance
10-17	2550	(1400)	38	+8.44	
10-45 (A) (B)	2550	(1400)	0.5	-----	Deteriorated
10-51	2550	(1400)	1.0	-----	Deteriorated
10-56	2550	(1400)	3.0	-----	Completely oxidized
11-9	2550	(1400)	5.0	-0.1	Al ₂ O ₃ spalled
11-13	2550	(1400)	38.0	-2.49	
11-14 (A)	2550	(1400)	17.0	-3.42	One flaw lead to failure
11-14 (B)	2550	(1400)	38.0	-4.88	Has potential
11-16 (B)	2550	(1400)	17.0	-8.11	

Table VI
Oxidation Test Results
(Continued)

Spec. No.	Oxidation Temperature		Total Time (Hours)	% Weight Change	Remarks
	°F	°C			
11-18	2550	(1400)	38.0	+0.66	
11-29	2550	(1400)	3.0	-----	Sample erupted
11-37	2550	(1400)	1.0	-----	Deteriorated
11-38	2550	(1400)	1.0	-----	Badly oxidized
11-54	2550	(1400)	3.0	-49.35	
11-90	2550	(1400)	3.0	-26.64	
11-91	2550	(1400)	3.0	-42.72	
11-92	2550	(1400)	3.0	-39.37	
11-88 (A)	2550	(1400)	0.25	-----	Coating erupted
11-88 (B)	2550	(1400)	0.25	-----	Coating erupted
11-30 (A) (B)	2550	(1400)	3.0	-6.73	
12-38	3000	(1600)	3.0	+1.77	
12-39	3000	(1600)	3.0	-61.57	Badly deteriorated

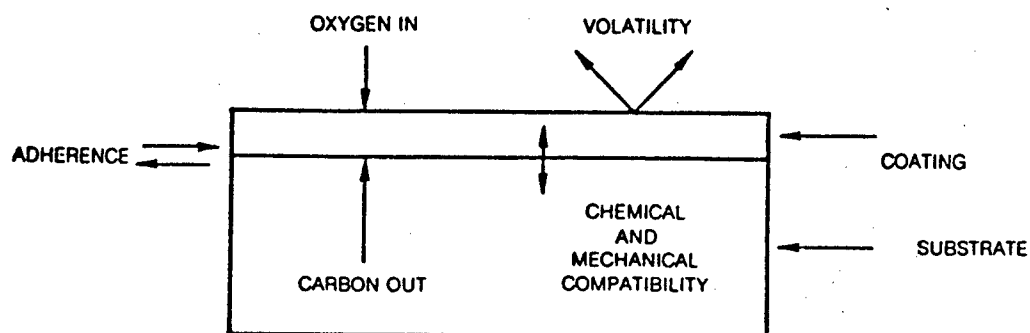
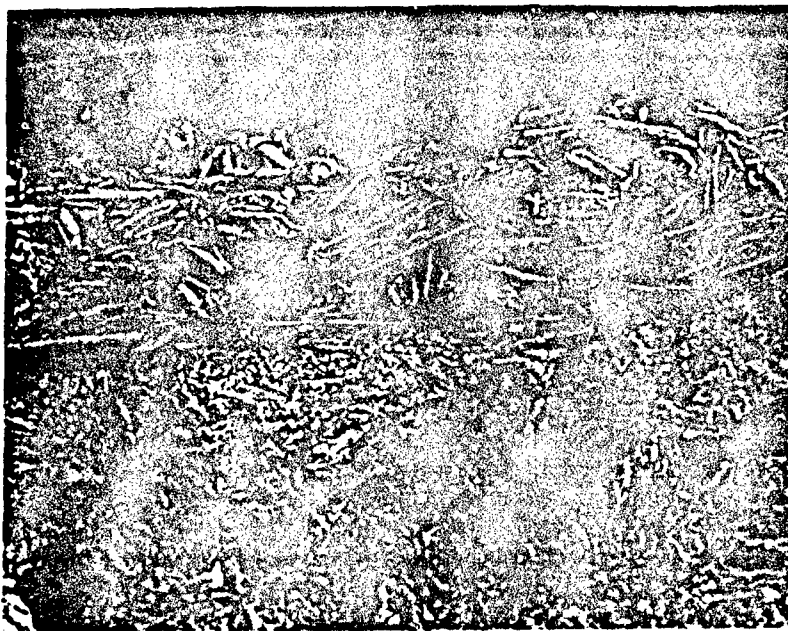
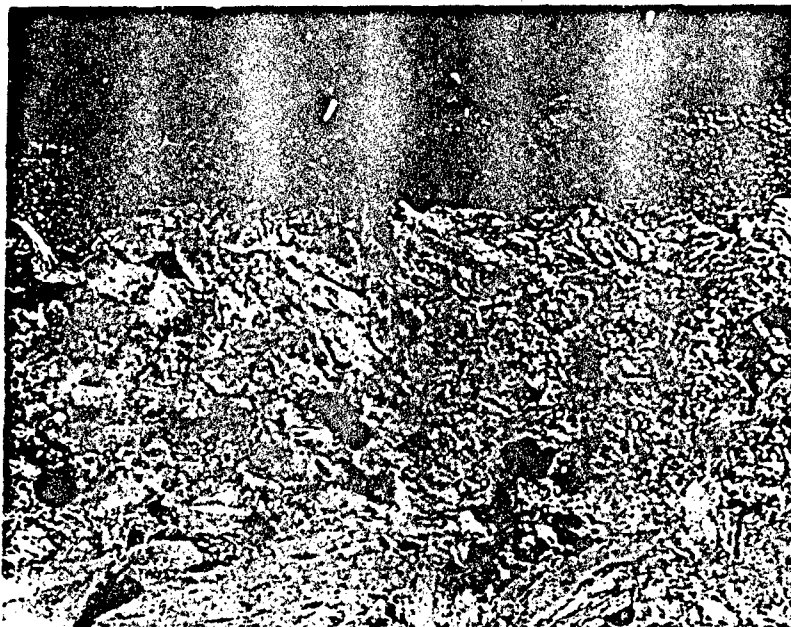


Figure 1: Factors Controlling the Oxidation Protection of Carbonaceous Substrates.



(A)



(B)

Figure 2: (A) Pitch-Graphite and (B) Pitch-Lampblack Coatings on ATJ Graphite. Mag. 500X

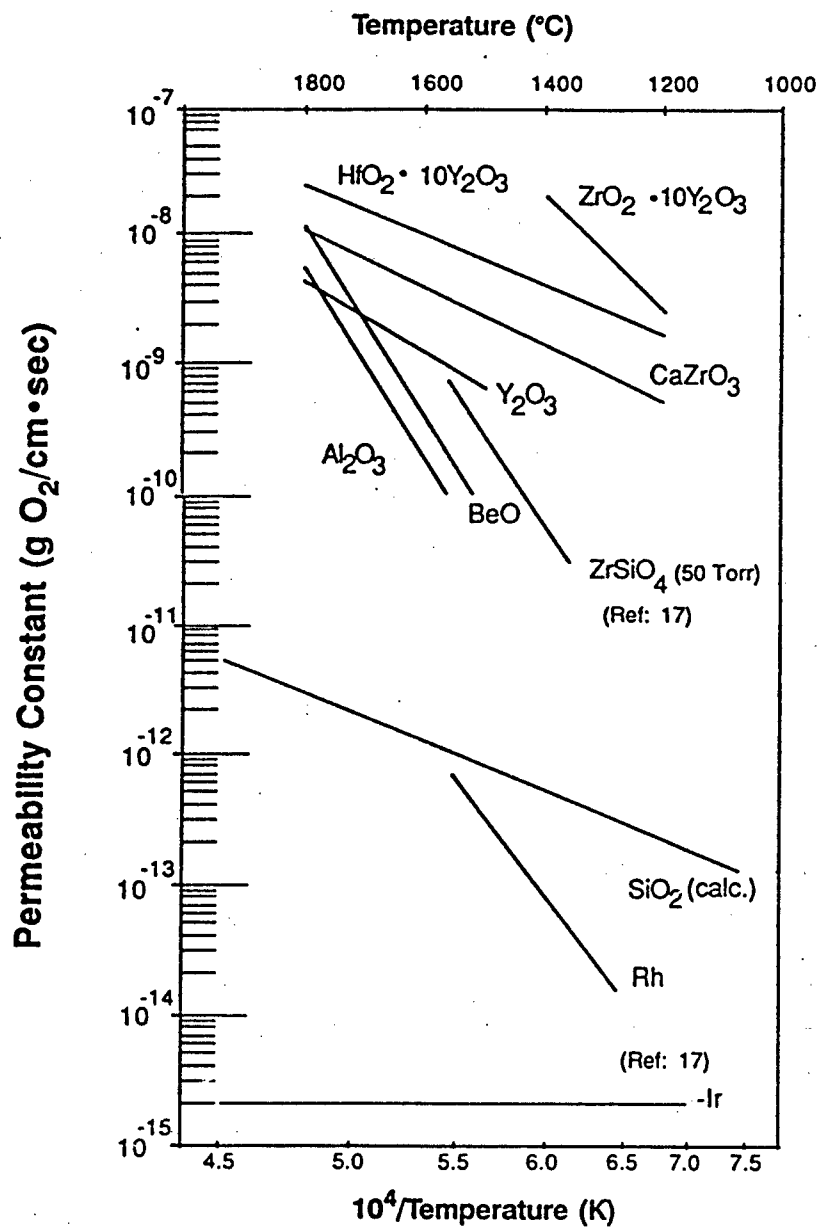


Figure 3: Range of Oxygen Permeability Through Several Oxides and Noble Metals at 0.21 Atm. Oxygen Partial Pressure. Reproduced from WL-TR-91-4006.

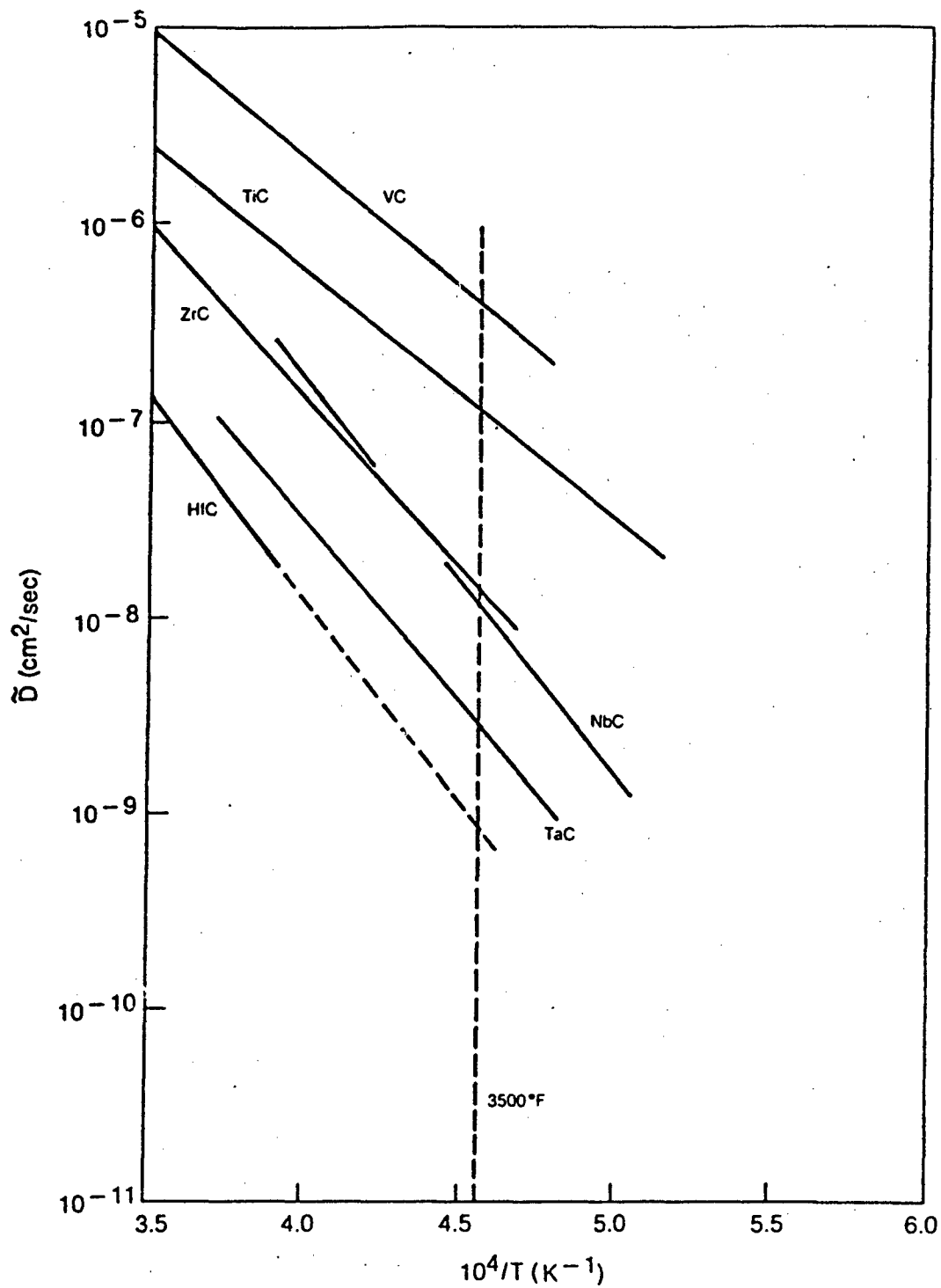


Figure 4: Carbon Diffusivity Determined by the Layer Growth Method. Reproduced from NADC-86087-60.

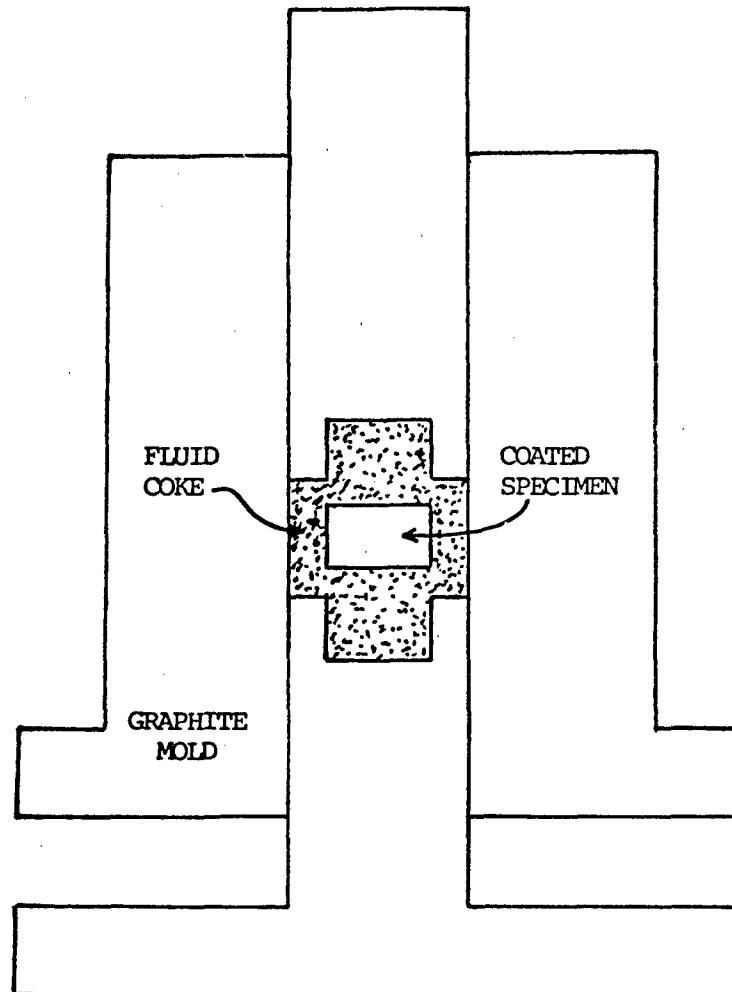
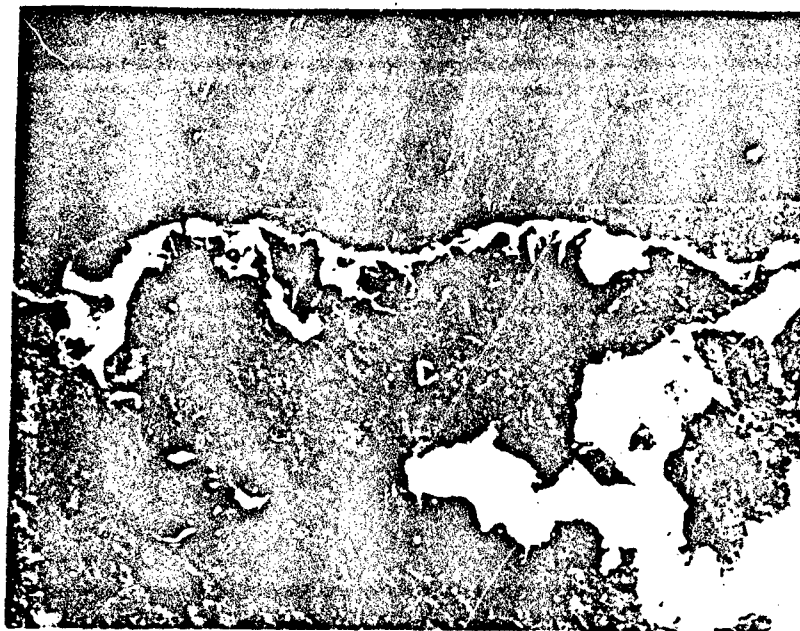


Figure 5: Quasi-Isostatic Hot Press Mold.



(A)

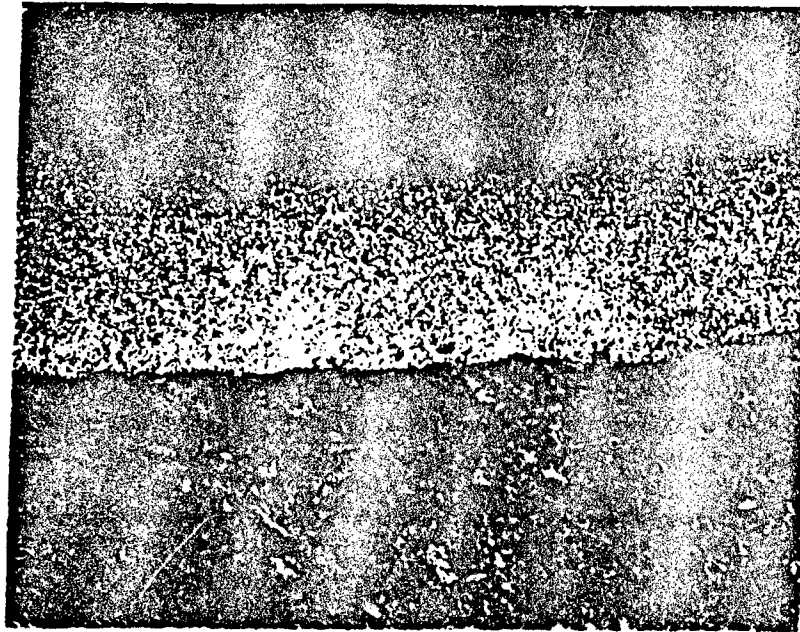


(B)

Figure 6: (A) Laser Fused HfSi_3 . Gray Phase is HfO_2 . (B) Lamellar Relationship of Two Hf-Si Phases. Lamellar Material is White in (A). Mag. of (A) is 500X.

<u>LAYER NO.</u>	FUNCTIONAL LAYERS
1	EROSION LAYER AND/OR
2	OXYGEN DIFFUSION LAYER
3	CARBON DIFFUSION LAYER
4	COMPLIANT LAYER
5	SUBSTRATE

Figure 7: Stacking Arrangement of Functional Layers.



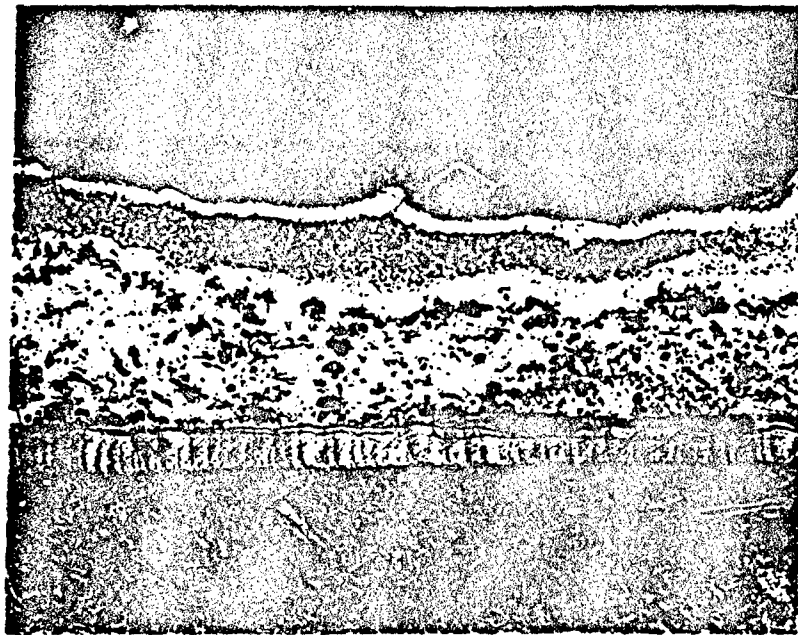
AlN

TaB₂

Pitch + Graphite

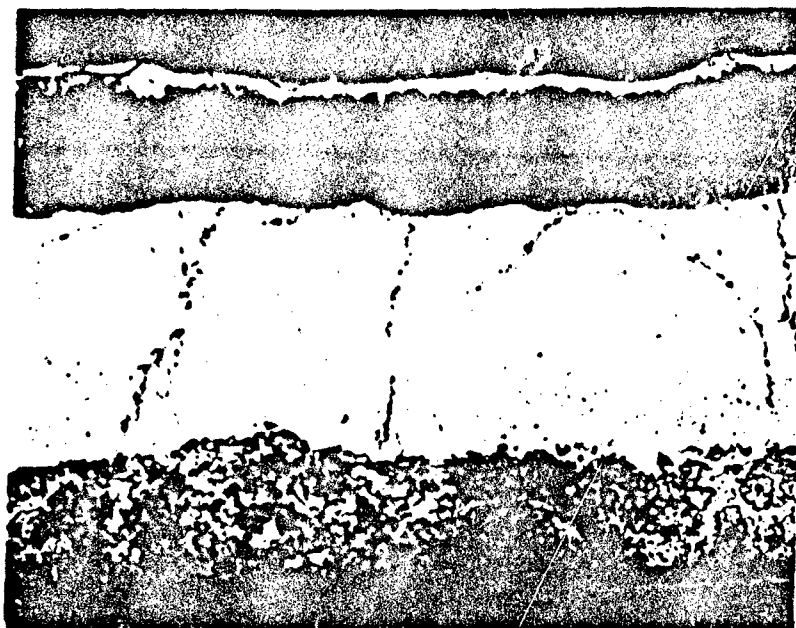
ATJ

Figure 8: Specimen 2-40 - HfO₂/AlN/TaB₂/Pitch + Graphite/ATJ.
Pitch + Graphite Compliant Layer is Evident Below TaB₂.
Mag. 100X



GRAFOIL
HfC (R)
HfO₂
HfC (R)
Hf
PGD
ATJ

Figure 9: Specimen 2-43 - HfO₂/Hf/PGD/ATJ. Reaction Areas and Delaminated PGD are Shown. Mag. 100X



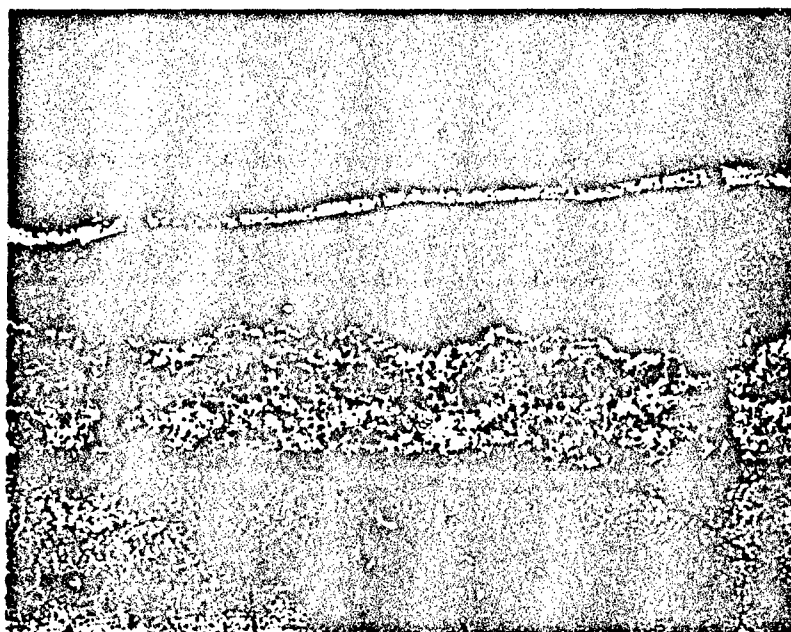
HfC (R)
HfO₂

TiN

HfO

PGD

Figure 10: Specimen 2-38 - HfO₂/TiN/HfO/PGD/ATJ. Reaction, Microcracked TiN, Delamination Between HfO and PGD. Mag. 100X



GRAFOIL

HfC (R)

HfO₂

Hf

CC

Figure 11: Specimen 4-92 - HfO₂/Hf/CC. Reaction, Major Cracks, Delaminated CC. Mag. 100X

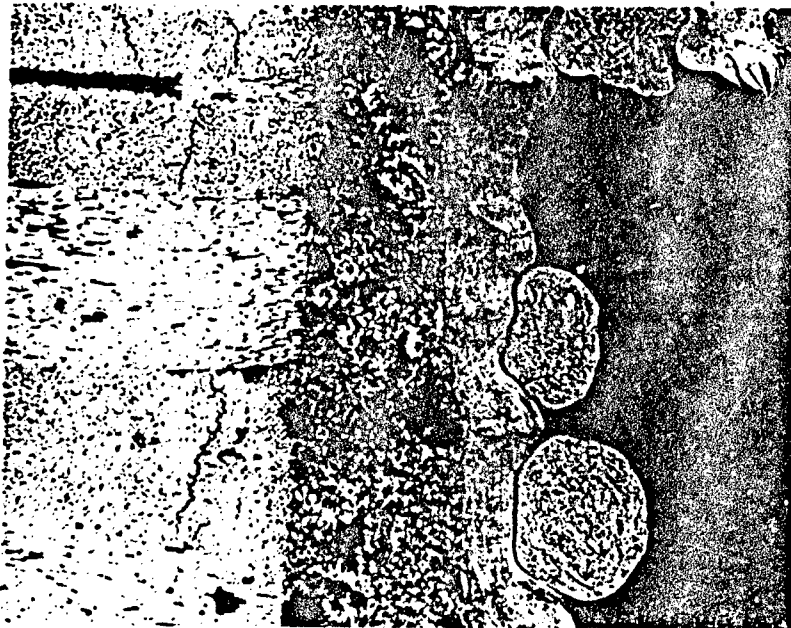


GRAFOIL

H4

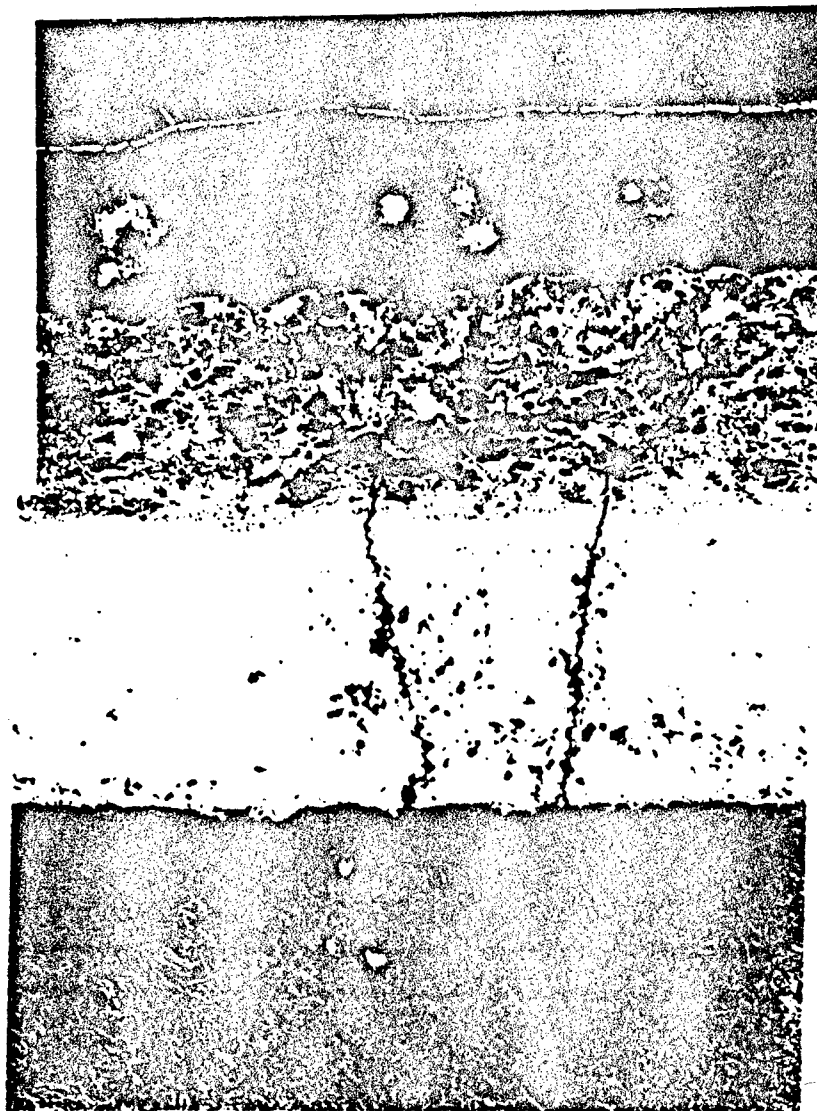
CC

(A)



(B)

Figure 12: Specimen 9-44 - H4/CC. (A) Top of Quasi-Isostatically Pressed Layer. (B) Side Region of Quasi-Isostatically Pressed Coating with Large Pores. Large Pellets are Fluid Coke Particles. Mag. 100X



HfC (R)

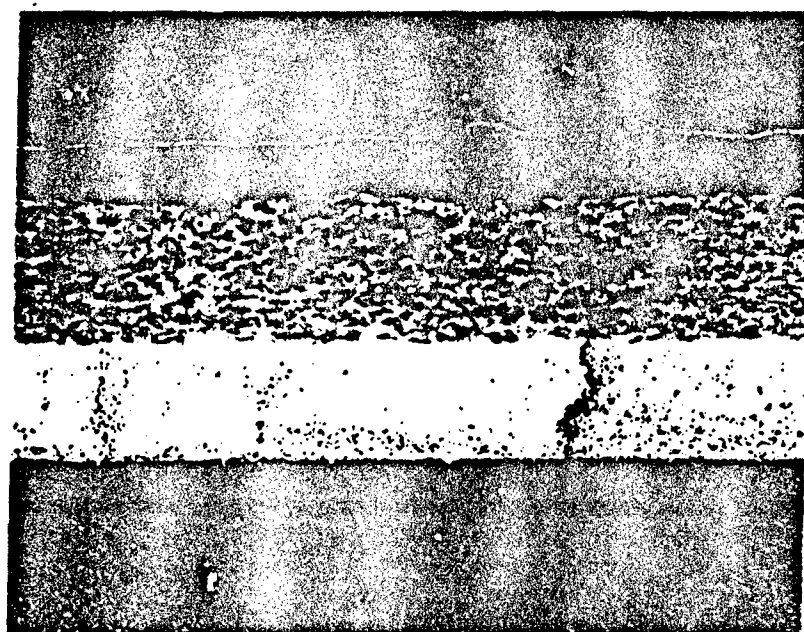
HfO₂

H₂

TaC

ATJ

Figure 13: Specimen 2-100 - HfO₂/H₂/TaC/ATJ. Reactions, Cracks in TaC Propagating into H₂. Mag. 100X



GRAFOIL
HfC (R)
HfO₂

T0

TaC

ATJ

Figure 14: Specimen 3-63 - HfO₂/T0/TaC/Pitch + Graphite/ATJ.
Reaction, Cracks in TaC Propagating into HfO₂.
Mag. 100X



HfC (R)

HfO₂

HfC (R)

SiC

H₂O

TaC

ATJ

Figure 15: Specimen 10-38 - HfO₂/SiC/H₂O/TaC/ATJ. Reactions, Cracks Propagating from TaC into H₂O. Mag. 500X



HfC (R)

HfO₂

HfC + HfO₂

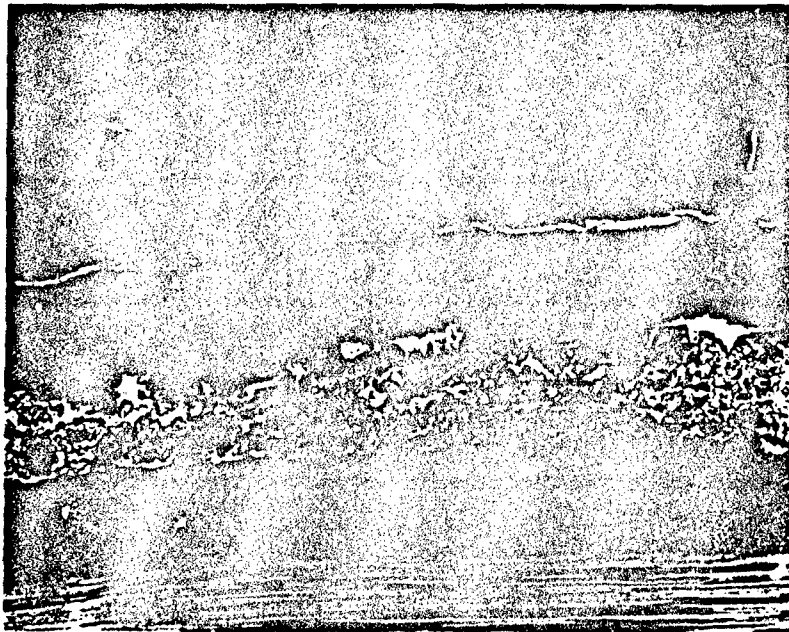
HfC

HfC + SiC

HO

ATJ

Figure 16: Specimen 7-12 - HfO₂/HfC + HfO₂/HfC/HfC + SiC/HO/ATJ. Reaction, Compositionally Graded, Very Few Cracks in Specimen. Mag. 500X



GRAFOIL

HfC (R)

HfO₂

AlN

H0

H5

CC

Figure 17: Specimen 8-27 - HfO₂/AlN/H0/H5/CC. Reaction, Microcracks from HfO₂ Terminated by AlN. Mag. 100X



HfO₂ + 15 w/o
SiC Whiskers

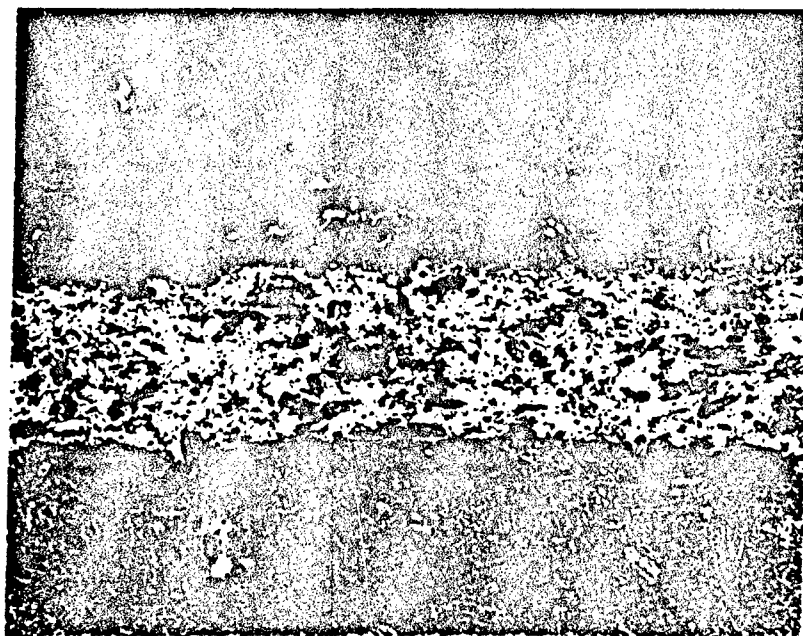
AlN

SiC

H5

CC

Figure 18: Specimen 8-87 - HfO₂ + 15 w/o SiC Whiskers/AlN/SiC/H5/CC. Reaction Between HfO₂ and SiC Whiskers, Crack-Free. Mag. 500X



GRAFOIL

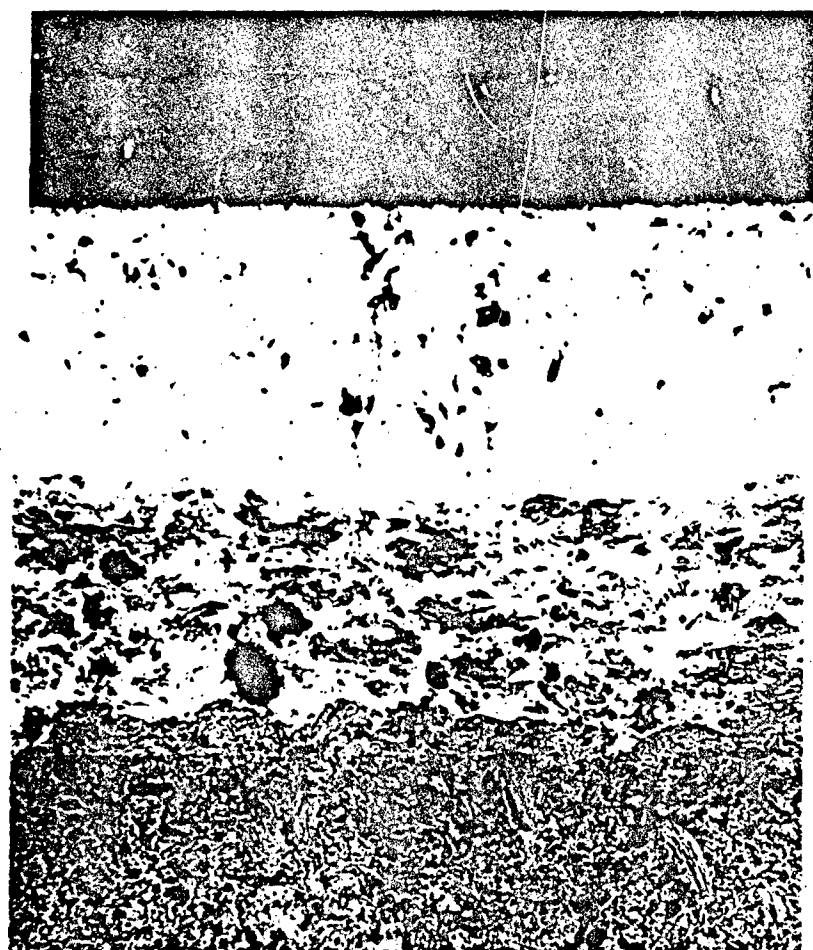
Y_2O_3

H1

Pitch + Graphite

ATJ

Figure 19: Specimen 2-42 - Y_2O_3 /H1/Pitch + Graphite/ATJ. Microcracks in Y_2O_3 Terminated by H1. Pitch + Graphite is Evident. Mag. 100X



Y₂O₃

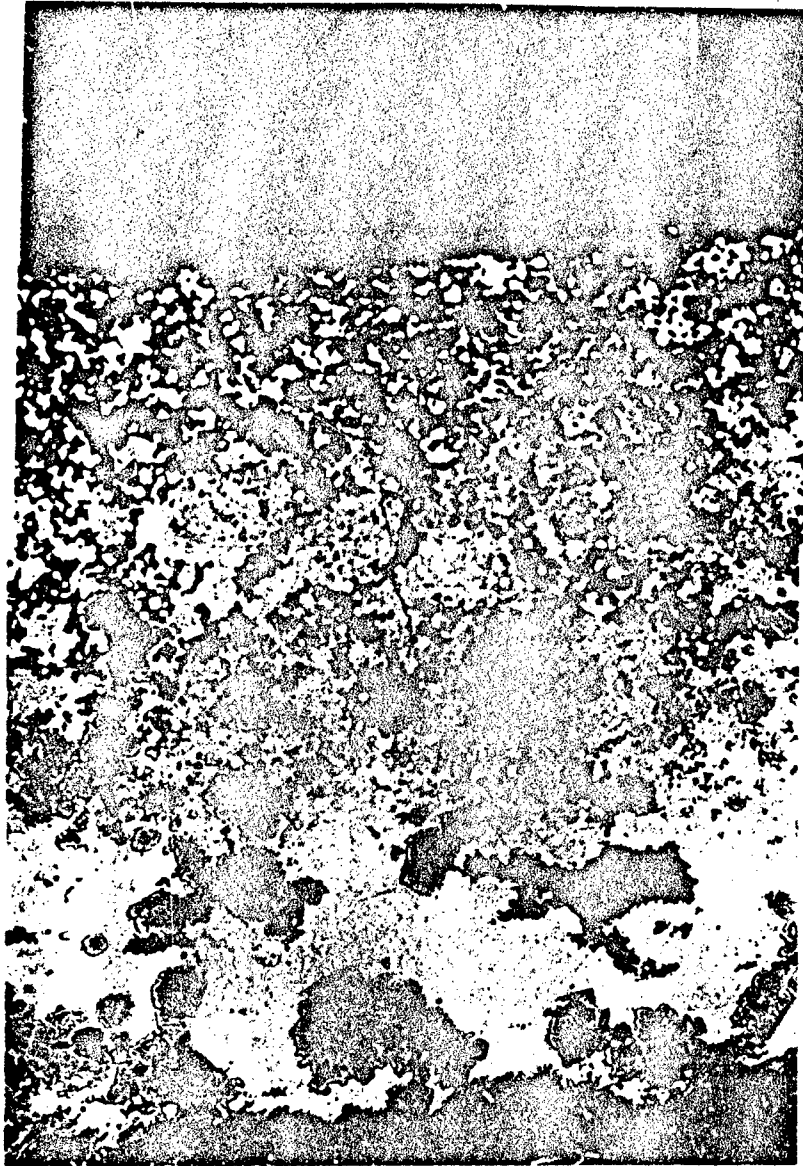
TaC

HfO₂

Pitch + Graphite

ATJ

Figure 20: Specimen 2-96 - Y₂O₃/TaC/HfO₂/Pitch + Graphite/ATJ.
Cracks Initiated at Y₂O₃ are Terminated by HfO₂.
Mag. 100X



Y_2O_3

$Y_2O_3 + TaC$

$TaC + SiC$

H0

ATJ

Figure 21: Specimen 7-4 - $Y_2O_3/Y_2O_3 + TaC/TaC + SiC/H0/ATJ$. Compositionally and CTE Graded. Cracks Initiated in Y_2O_3 Propagate into $Y_2O_3 + TaC$ where they Interact with TaC Particles. Mag. 500X



GRAFOIL

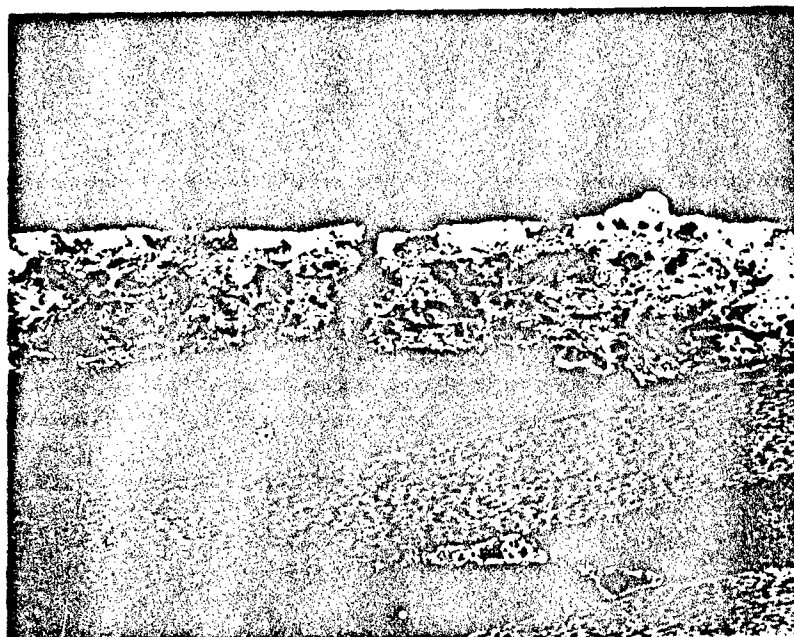
$Y_2O_3 + HfO_2$

$Y_2O_3 + HfC$
 $SiC + HfC$

HO

ATJ

Figure 22: Specimen 7-100 - $Y_2O_3 + HfO_2/Y_2O_3 + HfC/SiC + HfC/HO/ATJ$. Cracks Originate Internally at $Y_2O_3 + HfO_2/Y_2O_3 + HfC$ and Propagate to Exterior Surface of $Y_2O_3 + HfO_2$. Mag. 500X

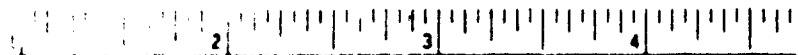
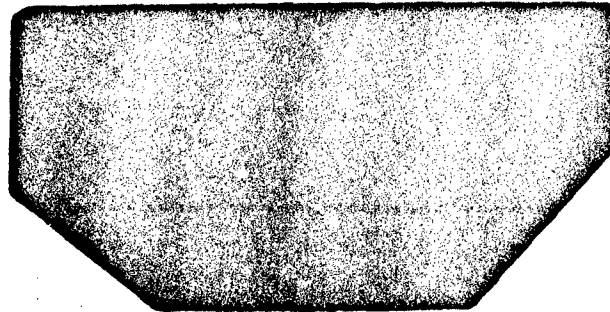


TiSi₂ + 5 w/o CrB₂

H5

CC

Figure 23: Specimen 5-61 - TiSi₂ + 5 w/o CrB₂/H5/CC. Specimen H5 on CC was Crack-Free Until TiSi₂ + 5 w/o CrB₂ was Added. Large Cracks Formed and Propagated to CC Causing Delaminations.



EXTRA MEASURE OF VALUE

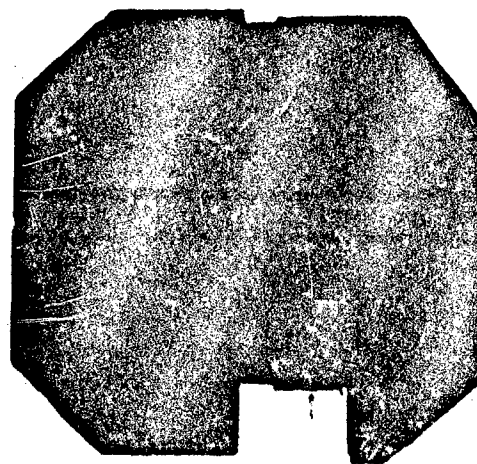


MACHINED GRAPHITE

PRECISION • QUALITY • PROMPT SERVICE

SPECIMEN 5-65G

(A)



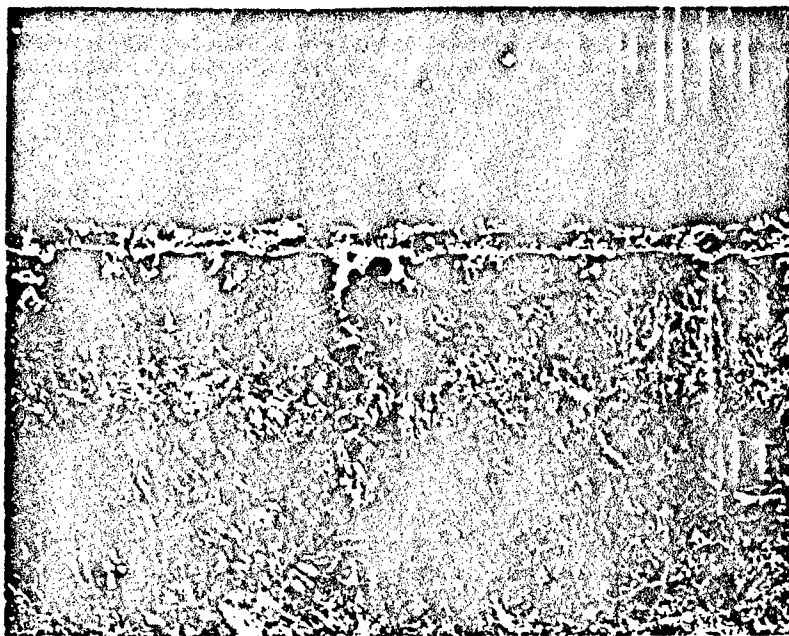
SPECIMEN 5-65E

(B)

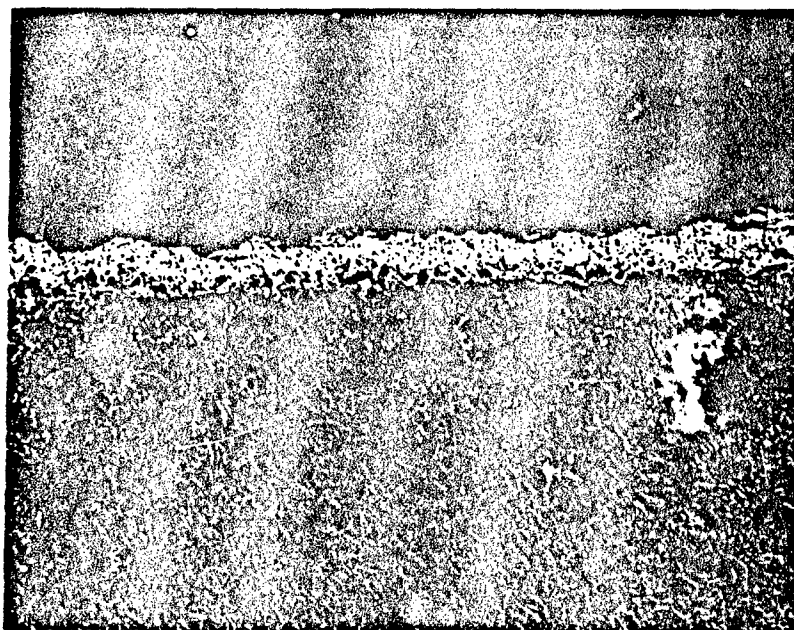
SPECIMEN 5-65D

(C)

Figure 24: Specimens 5-65G (A), 5-65E (B), and 5-65D (C). Oxidized CVD SiC Coatings on ATJ. (A) Coating Directly on ATJ Surface Resulting in Microcracks; (B) (C) Coating on Compliant Layers of SiC and SiC + TiC, Respectively.



(A)



(B)

Figure 25: Specimen 5-65D. (A) Compliant Layer and (B) CVD SiC Over Compliant Layer After 137 Hours at 1300°C.

BASIC DISTRIBUTION LIST

Technical Reports and Publications

Feb 1990

<u>Organization</u>	<u>Copies</u>	<u>Organization</u>	<u>Copies</u>
Defense Documentation Center Cameron Station Alexandria, VA 22314	12	Naval Air Propulsion Center Trenton, NJ 08623 ATTN: Library	1
Office of Naval Research Dept. of the Navy 800 N. Quincy Street Arlington, VA 22217 ATTN: Code 1131	3	Naval Civil Engineering Laboratory Port Hueneme, CA 94043 ATTN: Materials Div.	1
Naval Research Laboratory Washington, DC 20375 ATTN: Codes 6000 6300 2627	1 1 1	Naval Electronics Laboratory San Diego, CA 92152 ATTN: Electronic Materials Sciences Division	1
Naval Air Development Center Code 606 Warminster, PA 18974 ATTN: Dr. J. DeLuccia	1	Commander David Taylor Research Center Bethesda, MD 20084	1
Commanding Officer Naval Surface Warfare Center Silver Spring, MD 20903-5000 ATTN: Library Code R33	1 1	Naval Underwater System Ctr. Newport, RI 02840 ATTN: Library	1
Naval Ocean Systems Center San Diego, CA 92152-5000 ATTN: Library	1	Naval Weapons Center China Lake, CA 93555 ATTN: Library	1
Naval Postgraduate School Monterey, CA 93940 ATTN: Mechanical Engineering Department	1	NASA Lewis Research Center 21000 Brookpark Road Cleveland, OH 44135 ATTN: Library	1
Naval Air Systems Command Washington, DC 20360 ATTN: Code 310A Code 5304B Code 931A	1 1 1	National Institute of Standards and Technology Gaithersburg, MD 20899 ATTN: Metallurgy Division Ceramics Division Fracture & Deformation Division	1 1 1
Naval Sea Systems Command Washington, DC 20362 ATTN: Code 05M Code 05R	1 1		

Naval Facilities Engineering
Command
Alexandria, VA 22331
ATTN: Code 03 1

Commandant of the Marine Corps 1
Scientific Advisor
Washington, DC 20380
ATTN: Code AX 1

Army Research Office
P.O. Box 12211
Research Triangle Park, NC 27709
ATTN: Metallurgy & Ceramics
Program 1

Army Materials Technology Laboratory
Watertown, MA 02172-0001
ATTN: Research Program Office 1

Air Force Office of Scientific
Research
Building 410
Bolling Air Force Base
Washington, DC 20332
ATTN: Electronics & Materials
Science Directorate 1

NASA Headquarters
Washington, DC 20546
ATTN: Code RM 1

Defense Metals & Ceramics
Information Center
Battelle Memorial Inst.
505 King Avenue
Columbus, OH 43201 1

Oak Ridge National Laboratory
Metals and Ceramics Div.
P.O. Box X
Oak Ridge, TN 37380 1
Oak Ridge, TN 37380 1

Los Alamos Scientific Lab.
P.O. Box 1663
Los Alamos, NM 87544
ATTN: Report Librarian 1

Argonne National Laboratory
Metallurgy Division
P.O. Box 229
Lemont, IL 60439 1

Brookhaven National Laboratory
Technical Information Division
Upton, Long Island
New York 11973
ATTN: Research Library 1

Lawrence Berkeley Lab.
1 Cyclotron Rd
Berkeley, CA 94720
ATTN: Library 1

David Taylor Research Ctr
Annapolis, MD 21402-5067
ATTN: Code 281 1
Code 2813 1
Code 0115 1

4315DIST
April 1991

Supplemental Distribution List

Profs. G.H. Meier and F.S. Pettit
Dept. of Metallurgical and
Materials Eng.
University of Pittsburgh
Pittsburgh, PA 15261

Prof. H.K. Birnbaum
Dept. of Metallurgy
& Mining Eng.
University of Illinois
Urbana, IL 61801

Prof. H.W. Pickering
Dept. of Mat'l's Science & Eng.
The Pennsylvania State Univ.
University Park, PA 16802

Prof. D.J. Duquette
Dept. of Metallurgical Eng.
Rensselaer Polytechnic Inst.
Troy, NY 12181

Prof. D. Tomanek
Michigan State University
Dept. of Physics and Astronomy
East Lansing, MI 48824-1116

Dr. M. W. Kendig
Rockwell International Sci.Ctr.
1049 Camino Dos Rios
P.O. Box 1085
Thousand Oaks, CA 91360

Prof. R. A. Rapp
Dept. of Metallurgical Eng.
The Ohio State University
116 West 19th Avenue
Columbus, OH 43210-1179

Dr. R.D. Granata
Zettlemoyer Center for
Surface Studies
Sinclair Laboratory
Lehigh University
Bethlehem, PA 18015

Dr. G. D. Davis
Martin Marietta Laboratories
1450 South Rolling Rd.
Baltimore, MD 21227-3898

Dr. S.M. Lipka
Dept. of Ocean Engineering
Florida Atlantic University
Boca Raton, FL 33431-0991

Prof. J. Kruger
Dept. of Mat'l's Science & Eng.
The Johns Hopkins University
Baltimore, MD 21218

Dr. B.G. Pound
SRI International
333 Ravenswood Ave.
Menlo Park, CA 94025

Prof. C.R. Clayton
Department of Materials Science
& Engineering
State University of New York
Stony Brook
Long Island, NY 11794

Dr. J. W. Oldfield
Cortest Laboratories Ltd
23 Shepherd Street
Sheffield, S3 7BA, England

Ms. D.M. Aylor
Code 2813
David Taylor Research Center
Annapolis, MD 21402-5067

Prof. G. Simkovich
Dept. of Materials Sci. & Eng.
The Pennsylvania State Univ.
University Park, PA 16802

Dr. P.S. Pao
Code 6303
Naval Research Laboratory
Washington, D.C. 20375

Dr. N.S. Bornstein
United Technologies Research
Ctr.
East Hartford, CT 06108

Dr. B.A. Shaw
Dept. of Eng. Sci. & Mechanics
228C Hammond Building
The Pennsylvania State University
University Park, PA 16802-1484

Prof. R. M. Latanision
Massachusetts Inst. of Tech.
Room 8-202
Cambridge, MA 02139

Dr. R. E. Ricker
National Institute of Standards
and Technology,
Bldg. 223, Room B-266
Gaithersburg, MD 20899

Dr. F.B. Mansfeld
Dept. of Materials Science
University of Southern California
University Park
Los Angeles, CA 900889

Dr. W. R. Bitler
Dept. of Materials Sci. and Eng.
115 Steidle Building
The Pennsylvania State University
University Park, PA 16802

Dr. S. Smialowska
Dept. of Metallurgical Eng.
The Ohio State University
116 West 19th Avenue
Columbus, OH 43210-1179

Dr. R. V. Sara
Union Carbide Corporation
UCAR Carbon Company Inc.
Parma Technical Center
12900 Snow Road
Parma, Ohio 44130

Prof. M.E. Orazem
Dept. of Chemical Engineering
University of Florida
Gainesville, FL 32611

Prof. J. O'M. Bockris
Dept. of Chemistry
Texas A & M University
College Station, TX 77843

Dr. V. S. Agarwala
Code 6062
Naval Air Development Center
Warminster, PA 18974-5000

Prof. Harovel G. Wheat
Dept. of Mechanical Engineering
The University of Texas
ETC 11 5.160
Austin, TX 78712-1063

Prof. S. C. Dexter
College of Marine Studies
University of Delaware
700 Pilottown Rd.
Lewes, DE 19958

Prof. R.P. Gangloff
Dept. of Materials Science &
Eng.
Thornton Hall
University of Virginia
Charlottesville, VA 22903-2442

Dr. Wayne C. Tucker
Dept. of Ocean Engineering
University of Rhode Island
Kingston, R.I. 02881

Mr. M. M. Opeka
Code K22
Naval Surface Warfare Center
Silver Spring, MD 20903-5000

Dr. E. McCafferty
Code 6322
Naval Research Laboratory
Washington, D.C. 20375-5000

Dr. R.L. Jones
Naval Research Lab. (Code 6179)
Washington, D.C. 20375-5000

**END
FILMED**

DATE:

4-93

DTIC